MEMOIRS OF THE FACULTY OF SCIENCE, KYOTO UNIVERSITY, SERIES OF GEOL. & MINERAL.,
Vol. LV. No. 1-2, pp. 57-123, 1990

Block Structure Bounded by Active Strike-slip Faults in the Northern Part of Kinki District, Southwest Japan

By

Ikuo KATSURA

(Received November 1, 1989)

Abstract

Geological and geophysical surveys were carried out to discover the hidden active faults and to estimate the dimensions of fractured zone in the northern part of Kinki district, southwest Japan. Combining the geological and geophysical methods was effective to these purposes. In the geological survey, the attention was paid to the distribution of artesian springs except for the lineaments and the outcrops. In the geophysical survey, ELF-magnetotelluric and radioactive (γ-ray) methods were principal. Gravity method was applied to the sedimentary basins. The surveyed areas were distributed widely in the expected traces of major active faults beyond their terminals.

The results show that the major active strike-slip faults, such as the Yamasaki, the Jumantsuji, the Mitoke, the Yabu-Yagi and the Yamada faults, extend and continue each other through the undiscovered and fault-hidden areas. The newly discovered fracture named the Ute fault is considered to be a tectonic boundary between the Kinki and the Chugoku districts. The resistivity structures of the known active faults, such as the Hanaori, the Mikata and the Yanagase faults, are also confirmed. After these surveys, the pattern of active strike-slip faults suggests that the conjugate set of major strike-slip faults makes domains of land-mass called tectonic block. The Tamba block, which is enclosed by the chain of the Ute, the Yamasaki, the Jumantsuji, the Arima-Takatsuki, the Mitoke and the Yabu-Yagi faults, is a typical example.

In the central part of Kinki district, the reverse type of active north-south striking faults is a common feature. The Miyakata fault, which is an example of this type parallel to the Ikoma fault, has a vertical-slip of 200 m or more estimated from the gravity measurements. This fault could be assumed to be a part of the block boundary.

After comparison of major active faults, seven tectonic blocks are tentatively recognized in the region to the north of the Median Tectonic Line (MTL). The historical large earthquakes, of magnitude above 5.5, have occurred at and near the block boundaries.

Two active chains of block boundaries through historical ages could be recognized as convergence lines of the stress field. One extends from the Mikata-Hanaori fault towards the MTL through the Obaku fault and the Ikoma or the Miyakata fault. The other stretches from the Yanagase fault to the Ise-Bay fault through the Yoro fault. These active chains are situated in both outsides of the blocks composed of a granitic basement. The blocks between these chains are quiet in the intra-block micro-seismicity, but the exterior blocks composed of old and hard sedimentary basement are active.

1. Introduction

The northern part of Kinki district, southwest Japan, is characterized by a dense distribution of active faults which have displaced in the Quaternary period (RESEARCH GROUP FOR ACTIVE FAULTS [hereafter called R.G.A.F.], 1980). The major active faults in this region are shown in Fig. 1. There are two patterns of fault strikes making a conjugate set; one is WNW-ESE to NNW-SSE as left-lateral and the other is NNE-SSW to ENE-WSW as right-lateral. The examples of the former are the Yamasaki, the Yagi-Yabu and the Mitoke faults, and those of the latter are the Hanaori and the Yamada faults, the Arima-Takatsuki Tectonic Line (ATL) and the Rokko fault system (R.G.A.F., 1980). The N-S striking faults are mainly

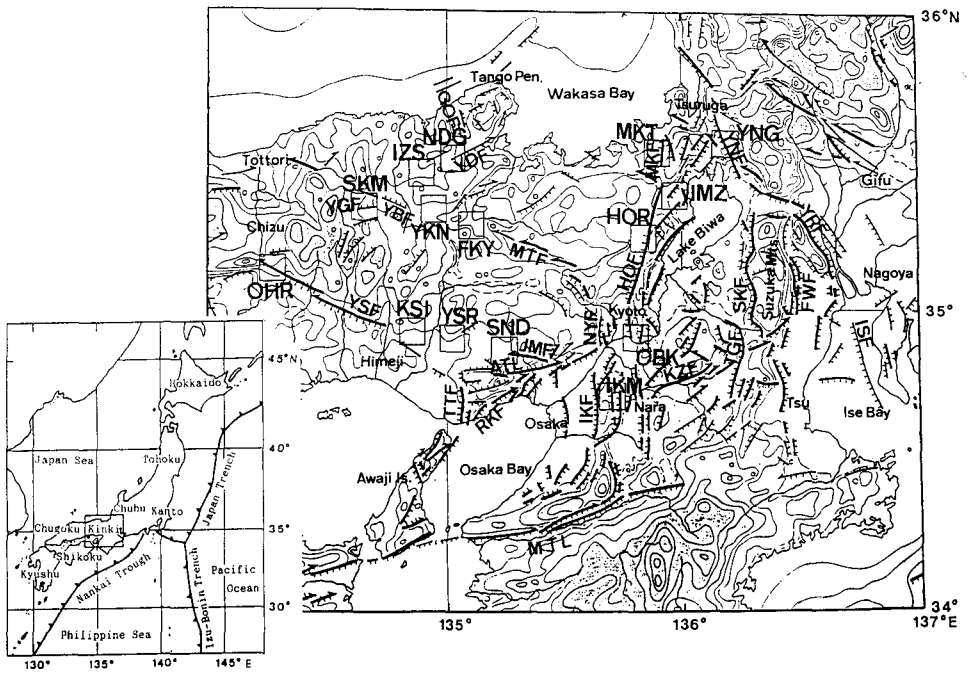

Fig. 1. Distribution of major active faults in the northern part of Kinki district, southwest Japan (after R.G.A.F., 1980) and surveyed areas (squares). Active faults are shown by bold line with strike-slip or downthrown direction. YSF: Yamasaki fault, ATL: Arima-Takatsuki Tectonic Line, JMF: Jumantsuji fault, RKF: Rokko fault system (Gosukebashi, Suwayama and Suma faults), TTF: Takatsukayama fault, YGF: Yagi fault, YBF: Yabu fault, MTF: Mitoke fault, NYF: Nishiyama fault, YDF: Yamada fault, GOF: Gomura fault, HOF: Hanaori fault, MKF: Mikata fault, IKF: Ikoma fault, KZF: Kizugawa fault, TGF: Tongu fault, SKF: Suzuka fault, FWF: Fujiwaradake fault, YNF: Yanagase fault, YRF: Yoro fault, ISF: Ise-Bay fault, MTL: Median Tectonic Line. YSR: Yashiro, KSI: Kasai, SND: Sanda, SKM: Sekinomiya, IZS: Izushi, NDG: Nodagawa, YKN: Yakuno, FKY: Fukuchiyama, OHR: Ohara, HOR: Hanaori, IMZ: Imazu, MKT: Mikata, YNG: Yanagase, OBK: Obaku, IKM: Ikoma areas.

reverse (or thrust) type and an example is the Ikoma fault.

The regional difference in fault type is pointed out in the north of the Median Tectonic Line (MTL); the conjugate system is predominant in the northwestern part, and the N-S striking reverse faults are remarkable in the central part (HUZITA *et al.*, 1973). The central part is often called the Kinki triangle area which is enclosed by the Osaka Bay-Tsuruga line, the Tsuruga-Ise Bay line and the MTL (HUZITA, 1969).

Tectonic stress appears in the distribution of active faults and the focal mechanism of earthquakes. The conjugate system and the N-S striking reverse faults are concordant with the direction of maximum pressure axis estimated from focal mechanisms of shallow earthquakes. The horizontally E-W to ESE-WNW compressional field is predominant in the north of the MTL (ICHIKAWA, 1971; NISHIDA, 1973; KISHIMOTO and NISHIDA, 1973). The strike-slip type of focal solution dominates in general, especially in the northwestern region of Kinki district, but the reverse type occasionally appears in the Kinki triangle area (ITO and WATANABE, 1977; OHKURA, 1988). The stress field is related to the westward subduction of the Pacific plate (HUZITA *et al.*, 1973).

Active faults were discovered by the lineament of topography using aerial photography and by the field survey for fault outcrops (R.G.A.F., 1980). The distribution of epicenters of micro-earthquakes which concentrate at these lineaments is also useful (HUZITA *et al.*, 1973; OIKE, 1976). Most of the active faults extend for several tens of kilometers. In general, the reverse type is rather shorter than the strike-slip type (Fig. 1). The Yamasaki, the ATL and the Hanaori faults are the examples of very long faults. The faults disappear gradually at their both ends. The reason for this disappearance is attributed not only to the true termination but also often to the hidden feature of active faults in the topography and geological setting. The development of thick alluvium masks the lineament structure. Few occurrences of micro-earthquakes also make the discovery of active fault to be difficult.

Techniques of geophysical exploration are effective to discover the hidden active faults. Attempts to trace the active faults in hidden areas (Fig. 1) have been carried out by using geophysical techniques associated with geological survey. The main techniques used were ELF-magnetotelluric (ELF-MT) sounding, radioactive method and geological field survey. The associated methods were the survey for hot and cold artesian springs and the gravity method. Some extensions of the active faults were discovered in the hidden areas. Results of the surveys were partly reported (MOGI *et al.*, 1985a, b; NISHIMURA *et al.*, 1985, 1986; KATSURA *et al.*, 1986, 1987a, 1989; YAMADA *et al.*, 1989; NISHIDA *et al.*, 1990). In this paper, all the facts obtained are compiled and a tectonic explanation for the active fault systems in the northern part of Kinki district is given.

2. Geological and Geophysical Surveys of Active Fault

The definition of active fault is given as follows; (1) the displacement occurred in the Quaternary period, (2) the displacement is repeatable, and (3) the displacement remains in a future possibility (R.G.A.F., 1980). The investigation of active fault is, in general, carried out by geomorphological and geological methods. The aerial photography is first employed and the lineament of topography is noticeable. The fault scarp and the displacement by faulting are next surveyed. The geological survey of fault outcrops is also included in this step.

The dimensions of fracture zone and the activity of faulting must be estimated for disaster prevention and earthquake prediction. The geophysical exploration techniques including seismic, gravimetric, electric and electromagnetic methods are valuable in these purposes. The seismicity, especially of micro-earthquakes, is also valuable. The records of historical earthquakes around the active fault must be referred for the estimation of recurrence time of faulting. This is most important in the earthquake fault. The Research Group for Active Faults compiled and catalogued the active faults in Japan with the rank of certainty and the degree of activity (R.G.A.F., 1980).

The distribution of active faults is most dense in the northern part of Kinki district (R.G.A.F., 1980). The map of active faults shows that the continuity of active faults is excellent in this area (Fig. 1). Some gaps in the continuity are, however, noticed. In the northwestern part of Kinki district, the strike-slip fault systems is abundant, but the gaps of continuity are found between the Yamasaki fault and the ATL, between the Yagi-Yabu and the Mitoke faults, and so on. The gaps are often located in the terrace and the alluvial plain. These gaps could be corresponding to the hidden areas of the active faults.

The surveys have performed to make clear the existence and continuity of active faults in the gap areas (Fig. 1). The geological survey especially for finding the fault outcrops was made in the mountain passes and the terrace scarps. The principal techniques used were the geophysical ones because of the specific conditions of the surveyed areas. Techniques applied to the fault-hidden areas are described in the followings with some examples:

2.1. Geological Survey

Surface geological survey is the first step of the series of the following geophysical surveys. The geological survey was attempted to discover the outcrops of fault at the mountainous area, pass, cliff and road cutting. The geomorphological features especially as lineament and fault scarp should be noticed. In the plain, the distribution of hot and cold artesian springs gives information on the location of hidden active fault. The artesian springs, especially containing H_2CO_3 and Cl, are located

along the active fault for many cases (KOIZUMI *et al.*, 1986); this phenomenon is caused by the presence of fissure water in the pores of fractured zone of fault. Their positions are less on the main fracture zone than on the auxiliary faults.

The Yagi fault is the western extension of the Yagi-Yabu fault and is a geologic boundary having an E-W strike and a length of about 20 km (Fig. 1). In the northern side, the Hokutan group composed of Miocene volcanics, volcaniclastic deposits and sediments is exposed (WADATSUMI and MATSUMOTO, 1958). In the southern side, the serpentinite body is extended. The Yagi fault is mentioned to an active fault as second rank of the certainty by topographic lineament (R.G.A.F., 1980). The micro-seismicity never occurred along this fault (TOTTORI MICROEARTHQUAKE OBSERVATORY).

The survey on this fault was planned to make clear the fracture zone (KATSURA *et al.*, 1987a). The surveyed area was in Sekinomiya, Hyogo Prefecture (Fig. 2). The geological survey was performed to find the fault outcrops and the artesian springs. The ELF-MT soundings were carried out at Kusade and Miyake areas. The radioactive method with γ-ray scintillation survey meter was adopted at Kusade, Kawaraba, Otani and Miyake areas. The survey lines of ELF-MT and radioactive methods were arranged to N-S direction acorss the expected trace of the fault. The results of geophysical explorations are described in the later. Lastly, the fracture zone is about 300 m of width with E-W strike. Individual fault lines are also traced as seen in the figure.

2.2. Radioactive method

The strength of radioactivity is dependent on the subsurface and basement rock types in the static sense. The additional effect should be imposed by the mobility of radioactive nuclides. The course of upward movement is deduced to be in the porous fracture zone of fault. In fact, the radon content of soil gas shows high level at the fracture zone (HATUDA, 1954). This fact is explained as the high mobility of gaseous radon. In this conception, we should measure the radioactivity caused by the daughter nuclides after radon. Nuclides in the uranium series are most abundant.

The exploration techniques in the present were reviewed in NISHIMURA and KATSURA (1990). Here, the γ-ray scintillation counter method was adopted. The instrument used is a γ-ray monitor called a survey meter. The scintillator is 1 inch diameter and length of NaI(Tl) crystal, and the γ-ray count rate as the exposure dose rate is read in rate meter in unit of micro-roentgen/hour (μR/h). The detector is inserted into the hole dug about 10 cm deep. After reading of rate meter holds the balance, twelve readings are recorded at intervals of 5 seconds. The mean value of ten readings except maximum and minimum values is adopted to the γ-ray intensity at the station. The γ-ray stations are arranged for making a survey

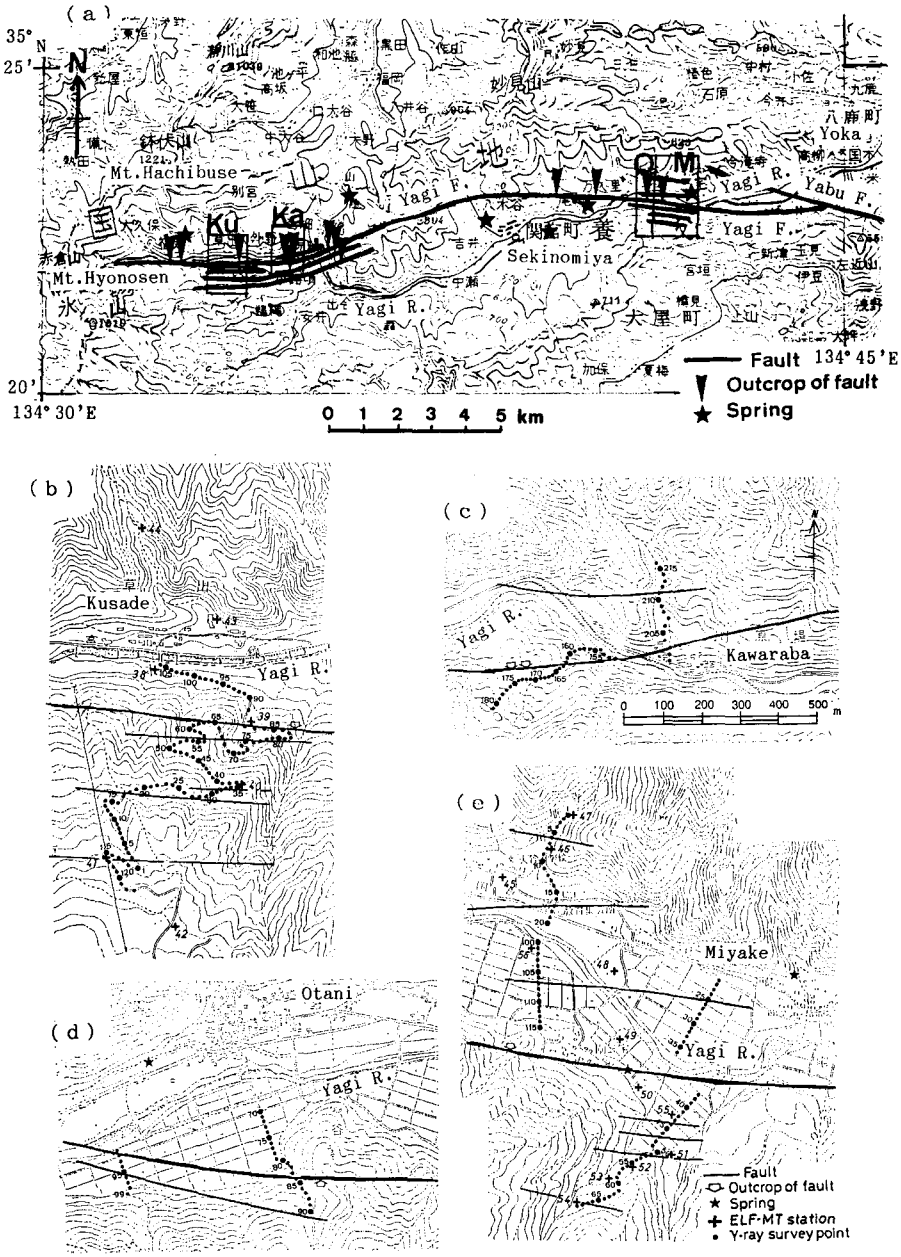

Fig. 2 Location of survey sites for the Yagi fault in Sekinomiya (after KATSURA *et al.*, 1987a). (a) Location of fault. Ku: Kusade, Ka: Kawaraba, O: Otani, M: Miyake areas. Detail maps are shown as (b), (c), (d) and (e), respectively.

line with spacing of 15 m. Survey lines are set across the assumed strike of the fault. The results are presented in a γ-ray profile with respect to the station array.

The γ-ray measured with a survey meter could not be distinguished its source nuclide. The knowledge of isotopic abundance and major elements in rocks introduces into an inference in which the uranium series and potassium are the major origin. Potassium is a major element in rock-forming minerals and ^{40}K is the source of γ-ray. The isotopic abundance of daughter nuclides after ^{222}Rn of the uranium series depends on the half-life or decay constant of each nuclide. In these nuclides, ^{214}Bi and ^{214}Pb are expected in the major sources of γ-ray.

The γ-ray survey using a multichannel spectrometer with NaI(Tl) scintillator reveals major sources of γ-ray in the natural environment. The instrument is usually called MCA. Three major peaks of energy spectrum of γ-ray correspond to ^{40}K, ^{214}Bi and ^{214}Pb (KATSURA *et al.*, 1986; KATSURA and NISHIMURA, 1987). A typical example can be seen in the results at the Obaku fault (Fig. 1) (KATSURA *et al.*, 1986). The fault runs along the eastern border of the southern Kyoto basin with about N-S strike (R.G.A.F., 1980) and cuts a part of the Quaternary Osaka group (UEJI, 1961). Several geophysical explorations on this fault were performed at Uji (KITSUNEZAKI *et at.*, 1971; MINO and TAKEUCHI, 1977; IRIKURA and KAWANAKA,

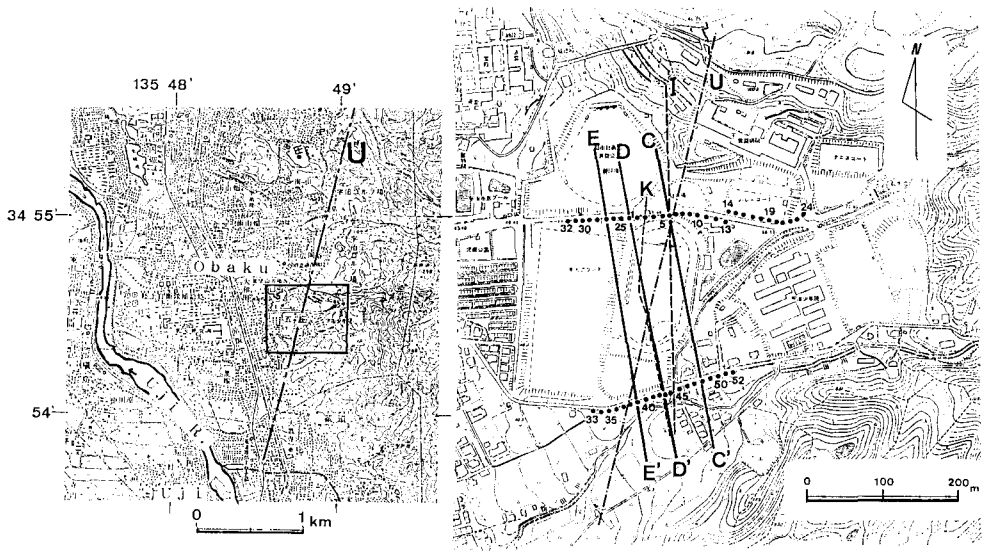

Fig. 3. Location of γ-ray survey at Obaku area, Uji City. U: Obaku fault after UEJI (1961), I: fault line inferred from seismic prospecting and microtremor measurements (IRIKURA and KAWANAKA, 1980), K: fault line inferred from electric resistivity method (KOBAYASHI *et al.*, 1984). C-C', D-D' and E-E' lines are three fault lines detected by KATSURA *et al.*, (1986).

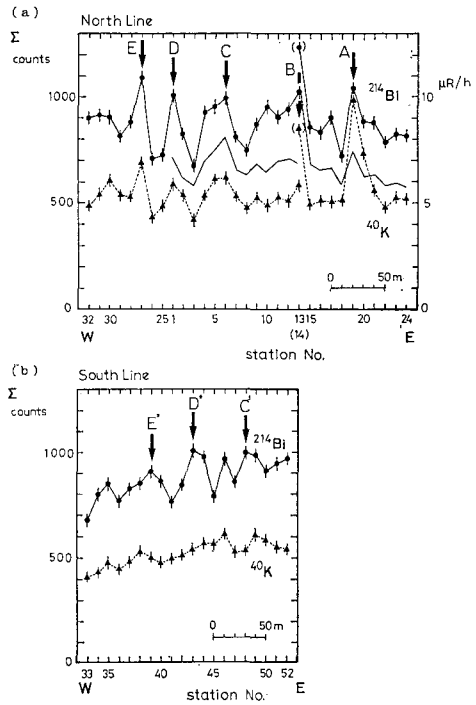

Fig. 4. γ-ray counts for 5 min. (live time) using MCA (ORTEC Model 7500 with NaI(Tl) scintillator) (after KATSURA *et al.*, 1986). Surveyed sites are shown in Fig. 3. Thin solid line in (a) shows the results measured by a TCS-121 γ-ray scintillation survey meter in unit of μR/h. Arrows C, D and E on north line (a) are correlated to C', D' and E' on south line (b), respectively. Three tie-lines C-C', D-D' and E-E' are fault planes, but arrows A and B on north line are doubtful.

1980; KOBAYASHI *et al.*, 1980, 1984). The displacement of basement as the uplift of east side is more than 150 m.

The survey lines and the results are shown in Fig. 3 and Fig. 4, respectively. The γ-ray counts caused by ^{214}Bi increase its level at the fracture zone of fault and the γ-rays from ^{40}K also increase at the same places. This tendency is also discovered at the Sabae fault, northwestern part of Chubu district (MINO, 1986).

The increase of ^{214}Bi could be explained by the high mobility of ^{222}Rn through fractures. The increase of ^{40}K may be attributed to the concentration in clay minerals at fault after the flow of water dissolving potassium. On the contrary, the associate peaks of γ-ray energy caused by ^{214}Bi are discovered near the peak of ^{40}K (OKABE *et al.*, 1988). According to this fact, the γ-ray counts of ^{40}K detected by NaI(Tl) multichannel analyzer include some contribution of ^{214}Bi.

In the case of Yagi fault at Sekinomiya (Fig. 1), the γ-ray survey lines were arranged to be across the expected traces of fault lines (see Fig. 2). The results are

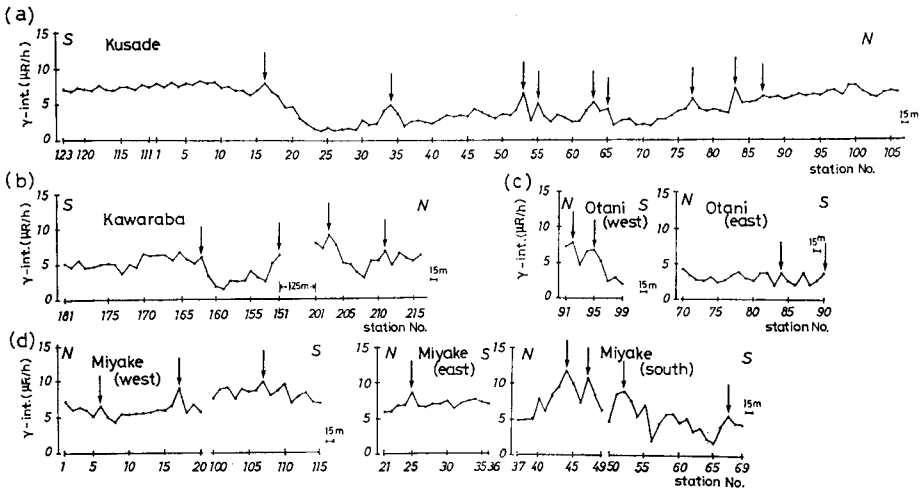

Fig. 5 γ-ray profiles of the surveyed lines across the Yagi fault at Sekinomiya (after KATSURA *et al.*, 1987a). Surveyed sites are shown in Fig. 2. Arrows show the possible positions of fault plane at surface. (a) Kusade, (b) Kawaraba, (c) Otani and (d) Miyake areas.

shown in Fig. 5. The peaks of γ-ray profiles suggest possible positions of the fault lines. The estimated traces of fault lines shown in Fig. 2 are the solutions after correlation among the γ-ray, the ELF-MT, the lineament and the outcrops.

2.3. ELF-Magnetotelluric Sounding

Magnetotelluric (MT) sounding is one of the electromagnetic exploration techniques to estimate resistivity structure of subsurface layers by measuring both electric and magnetic fields at the surface. Natural geomagnetic field is very noisy and has various components of frequency of its fluctuation by origin to origin. After the injection of magnetic field into the conductive earth from the space, the electromagnetic field propagates into deep-seated layer by the alternation of induced electric and magnetic fields. The energy reduction of electromagnetic field is dependent on its frequency. A lower frequency component of electromagnetic field has the information of deeper sub-surficial layer on the resistivity (or conductivity).

Basic theory of MT sounding was given by CAGNIARD (1953). Here, we assume that the earth is a semi-infinite body, electrically homogeneous and isotropic. When we could assume that the injection of magnetic field into the conductive earth from random orientation and that the receiver site is far enough from the source of electromagnetic noise, we could consider that the plane electromagnetic wave injects vertically. On these assumptions, we obtain a relation between resistivity, ρ_a (Ωm), and a perpendicular set of electric field, E_x (V/m), and magnetic field, H_y (A/m), as follows;

$$\rho_a = \frac{1}{\omega\mu}\left|\frac{E_x}{H_y}\right|^2 = \frac{1.26\times10^5}{f}\left|\frac{E_x}{H_y}\right|^2 \quad (1)$$

where μ (H/m) is magnetic permeability (of free space), ω (radian/s) and f (Hz) are angular velocity and frequency of electric and magnetic fields. ρ_a is called apparent resistivity of f Hz. The depth where the intensity of electromagnetic wave reduces to $1/e$ of intensity at the surface is called skin depth. The skin depth, δ (m), for f Hz wave is defined as

$$\delta = \sqrt{\frac{2\rho}{\omega\mu}} = 503\sqrt{\frac{\rho}{f}} \quad (2)$$

where ρ is resistivity of the semi-infinite layer in Ωm.

The necessary fieldwork is synchronous measurements of natural telluric current (electric field) and magnetic field in the perpendicular directions. The employed frequencies of the fluctuated magnetic field and the induced telluric current are in the ELF (extra low frequency) band. The ELF noises of electromagnetic wave are raised by the worldwide thunderstorms and maintained by the resonance of cavity composed of the conductive earth and ionosphere (OGAWA *et al.*, 1969, 1979). The characteristic frequencies are called the Schumann resonances. The MT method used ELF band is called the ELF-MT method.

In the ELF-MT method, three frequencies, 7.8, 14.0 and 20.4 Hz, of the Schumann resonances were employed. The VLF (very low frequency) signal of 17.4 kHz transmitted from Kariya, central Japan, is also received to estimate the resistivity of surface layer. The ELF-MT meter is composed of induction coils for ELF and VLF bands, a pair of electrodes, and two amplifier units for magnetic and electric fields (Fig. 6). Basic system of the meter used is the same as the instrument used by HANDA and SUMITOMO (1985) and MOGI *et al.* (1986). After the test of ELF noises, which are often influenced and obscured by the power line, using an oscilloscope, the amplified and band-passed signals are introduced into a handheld computer through an AD converter. The apparent scalar resistivity is immediately calculated by eq. (1). As the ELF noises are random noises in general, the apparent resistivities of repeating measurements (usually 30 times) for each frequency should make a log-normal distribution (MOGI *et al.*, 1986). Mean apparent resistivity on log-scale for each frequency is calculated after the statistical test by the way of Smilnov's rejection test. After the above procedures, we obtain four values of mean apparent resistivities on log-scale and of log-standard deviations for a perpendicular set of magnetic and electric fields.

The ELF-MT method in the survey of active faults is based on the fact that the fracture zone of active fault has a low resistivity value (ELECTROMAGNETIC

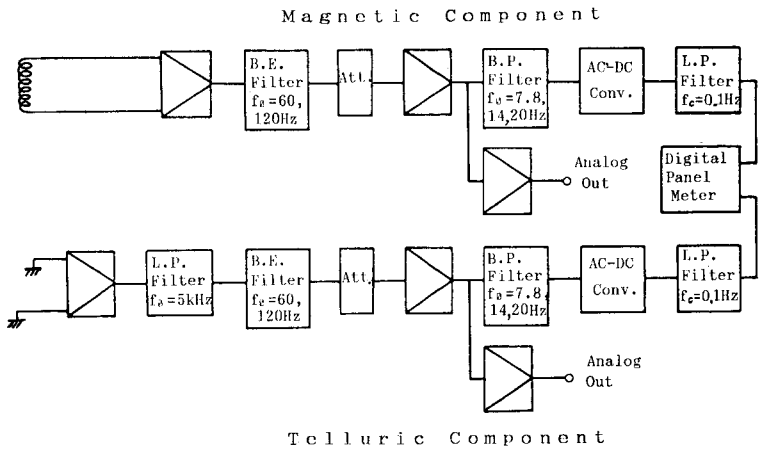

Fig. 6. Block diagram of ELF-MT meter. f_0 is the center frequency of band pass (B.P.) and band eliminate (B.E.) filters. f_c is the cut off frequency of low pass (L.P.) filter.

Research Group for the Active Fault [hereafter called E.R.G.A.F.], 1982). As the porosity of fracture zone is usually high, the voids are filled with partly ionized water in the case of wet climate. Then the resistivity of fracture zone reduces its value. When the ELF-MT stations were situated on a line across an active fault, we could get a relative change of apparent resistivities respect to the station array. The apparent resistivity of the station on fracture zone is relatively low.

A plot of apparent resistivities with respect to the distance between stations is called a profile of apparent resistivity. In the case of active fault, the fracture zone of low resistivity makes a two-dimensional structure with infinite elongation along the strike of fault. The measurement of TM-mode (transverse magnetic field) means the case in which the magnetic field is measured in the direction parallel to the strike of fault. The TE-mode (transverse electric field) measurement is the opposite case in which the electric field is measured in parallel direction to the strike. We could get a sharp and abrupt changes of apparent resistivity at the edges of fracture zone in the TM-mode profile (Vozoff, 1972; Strangway *et al.*, 1973; Reddy and Rankin, 1975; Handa and Sumitomo, 1985).

The diagnosis of the fault fracture zone is dependent on the apparent resistivity profile in TM-mode. When we could presume the strike of hidden fault, we arranged the TM mode measurement. On the contrary, when we had no presumption of fault strike, we arranged two sets of measurements exchanging the directions of magnetic and electric fields. The geometric mean resistivity calculated from two sets of measurements is often used for this case. Usually, N-S and E-W directions were adopted. The width of fracture zone is estimated from a pair of abrupt changes of apparent resistivity in an ideal TM-mode profile. As the low frequency electromag-

netic wave penetrates to deep, the depth of fracture zone is related to the lowest frequency showing low apparent resistivity. Furthermore, as the electromagnetic wave penetrates to deeper through the higher resistivity medium, the depth of fracture zone is also related to the value of resistivity.

The ELF-MT soundings across the Yagi fault were carried out in Kusade and Miyake areas (Fig. 2). The apparent resistivity profiles are shown in Fig. 7. The figure shows relatively clear separation of TM- and TE-modes. The case of E-W

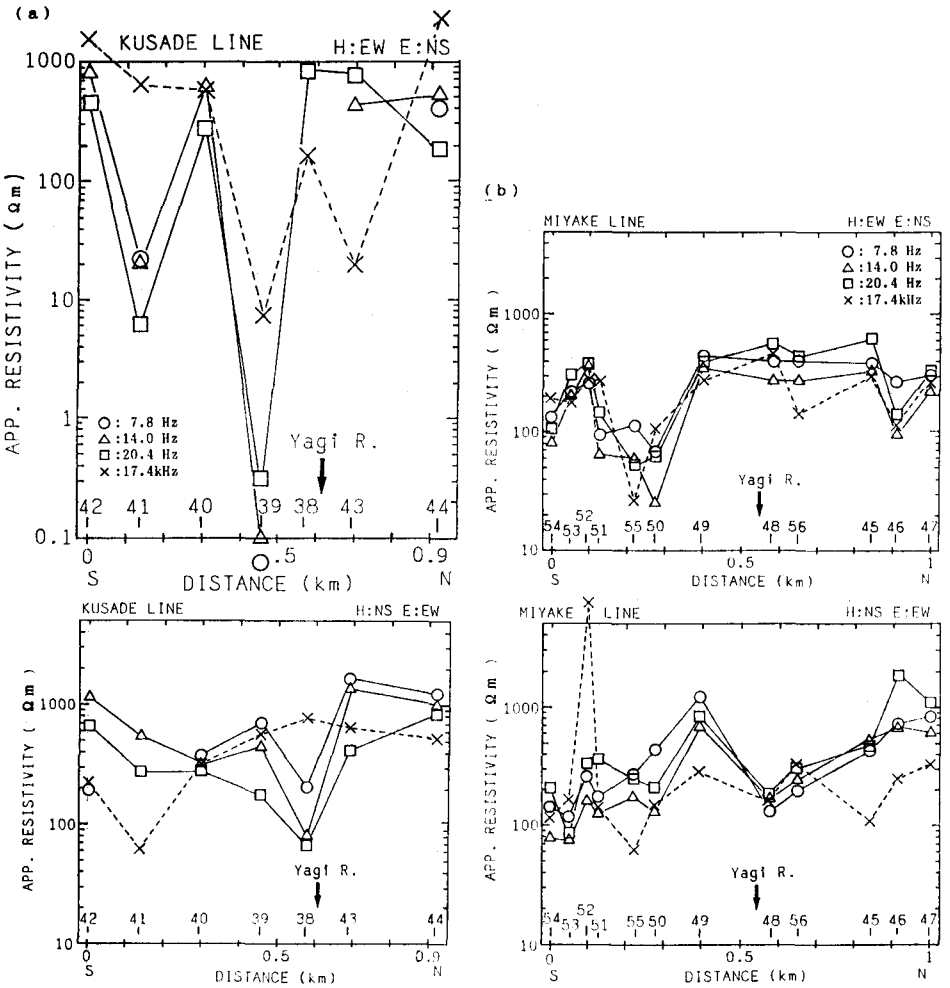

Fig. 7. N-S apparent resistivity profiles of ELF-MT soundings across the Yagi fault at Sekinomiya (modified from KATSURA *et al.*, 1987a). Surveyed sites are shown in Fig. 2. Distance is measured along N-S projection. (a) Kusade and (b) Miyake areas. Upper and lower correspond to TM- and TE-modes, respectively.

magnetic field can be presumed to be the TM-mode. Remarkable low apparent resistivities for the TM-mode are seen at the sites 38, 39 and 41 of the Kusade line and at the sites between 50 and 51 of the Miyake line. The horizontal extent of fracture zone can be interpreted to be the range between the sites 49 and 52 for the Miyake line. For the Kusade line, it is possible that the fracture zone separately runs at the sites 38 and 39 and at the site 41.

The resistivity structure of underground layers is estimated by one-dimensional and two-dimensional analyses. The one-dimensional analysis is an inversion problem and based on the assumption with two or three layers of laterally homogeneous media. As the ELF-MT method employs three frequencies of ELF-band and one frequency of VLF-band, we cannot assume a multi-layers model more than three. Let ρ_i and h_i be resistivity and thickness of the i-th layer, respectively. The bottom layer is semi-infinite; h_2 or h_3 are infinite on the two- or three- layers model. In the two-layers model, apparent resistivity is given by the following formulae (KAUFMAN and KELLER, 1981);

$$\begin{aligned} \rho_a &= \rho_1\{coth(-ik_1h_1+coth^{-1}\sqrt{\rho_2/\rho_1})\}^2 \qquad (\rho_2>\rho_1) \\ \rho_a &= \rho_1\{tanh(-ik_1h_1+tanh^{-1}\sqrt{\rho_2/\rho_1})\}^2 \qquad (\rho_2<\rho_1) \end{aligned} \tag{3}$$

where i is imaginary unit and k_1 is equivalent to wave number as $k_1=(1+i)/\delta_1$. In here, δ_1 is skin depth of the first layer. In the case of three-layers model, apparent resistivity is given by

$$\rho_a = \rho_1[coth\{-ik_1h_1+coth^{-1}\sqrt{\rho_2/\rho_1}\,coth(-ik_2h_2+coth^{-1}\sqrt{\rho_3/\rho_2})\}]^2 \tag{4}$$

for $\rho_3>\rho_2>\rho_1$. For $\rho_3<\rho_2<\rho_1$, substitute *tanh* for *coth* of eq. (4). We could obtain suitable formula to calculate apparent resistivity by substitution between *tanh* and *coth* according to the relation of inequality among resistivities of the layers. The master curve of apparent resistivity respect to the frequency is calculated from the subsurface model. The calculated apparent resistivities are fitted to the observed values by improving the model in the least-squares sense with taking account of log-standard deviation of observed values.

In the case of Yagi fault, the width of fracture zone is estimated to be about 300 m at Miyake (see Fig. 7). The vertical extent of fracture zone is estimated by the resistivity structure after one-dimensional and two-dimensional analyses of ELF-MT soundings. The one-dimensional analysis was adopted to the two survey lines at Kusade and Miyake. The solutions are presented in Fig. 8(a) and (b). For the Kusade line, the fracture zone extends under the sites 38, 39 and 41. For the Miyake line, the resistivity structure will be explained later.

Two-dimensional Analysis: This analysis was only applied to the surveyed line showing a typical mode separation such as the survey lines across the Yagi fault at

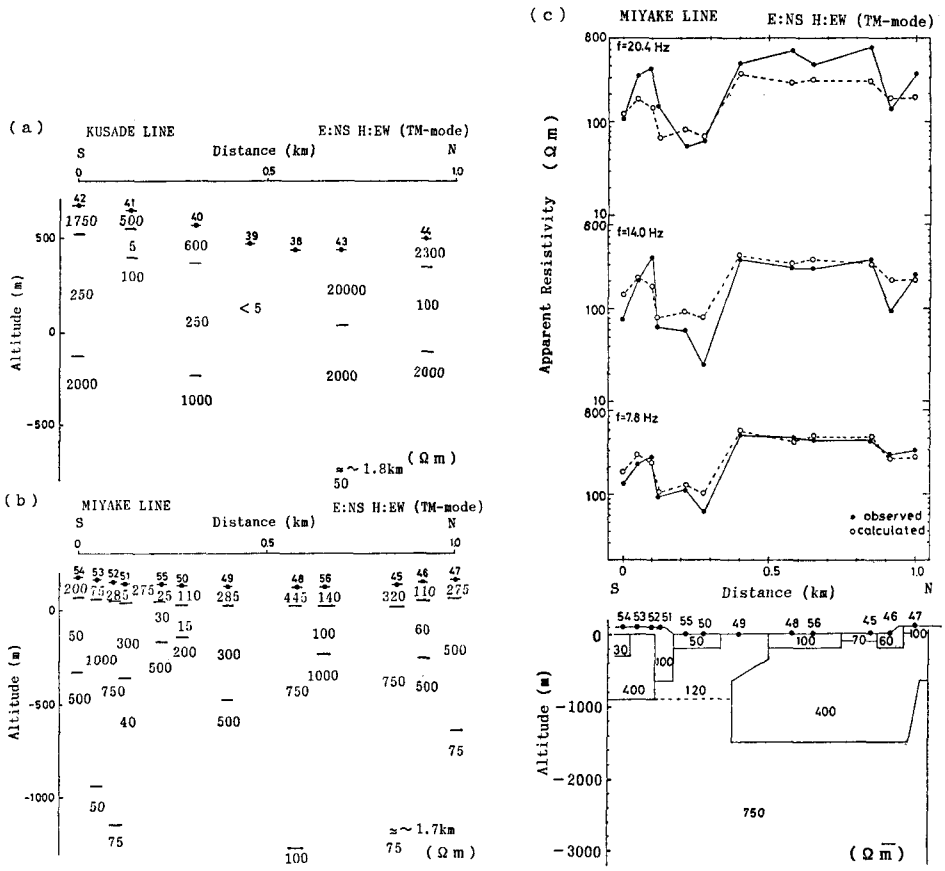

Fig. 8. N-S resistivity sections across the Yagi fault at Sekinomiya (modified from KATSURA *et al.*, 1987a). Surveyed sites are shown in Fig. 2. Distance is measured along N-S projection. (a) One-dimensional model (TM-mode) at Kusade. (b) One-dimensional model (TM-mode) at Miyake. (c) Two-dimensional model at Miyake with goodness of fitting for apparent resistivity of TM-mode.

Miyake (in this study) and the Hanaori fault (YAMADA *et al.*, 1989). The two-dimensional model is improved by try and error method to fit the observed apparent resistivities of TM-mode. The starting model is designed from the results of one-dimensional analysis especially of TE-mode, because the singularity of one-dimensional solution is less in the TE-mode than the TM-mode. The computer program used is based on the finite element method (FEM) of REDDY and RANKIN (1975). The shape of elements is triangular and the total number of elements is 1652.

The solution after the two-dimensional analysis is presented in Fig. 8(c) for the Miyake line across the Yagi fault. The goodness of fitting is also shown in the figure. Although there is a limitation on basement's resistivity which is uniform,

the figure clearly shows the horizontal contrast at the upper layer between the fracture zone and the unfractured outsides. The layers of 50, 100 and 120 Ωm under the sites between 49 and 51 correspond to the fracture zone. The resistivity contrast is more clear than that of the one-dimensional model (see Fig. 8(b)). The vertical extent of fracture zone, however, has a little uncertainty, because there is a limitation on the use of natural ELF band. The dimensions of fracture zone at Miyake is concluded to be about 300 m of width and 900 m or more of depth.

Tensor Impedance Method: In the Ohara area (Fig. 1), we attempted to discover the principal axis distribution of impedance tensor on anisotropic earth as the manner of VOZOFF (1972). The data processing, especially on the observed data selection, was based on the coherence functions defined by REDDY and RANKIN (1974). This method could only be applied to the area where the ELF-noises were very clear and not influenced by the artificial noises from the power line.

This method clarifies the horizontal heterogeneity of subsurface resistivity and the direction of elongated low resistivity zone. For this purpose, we measure simultaneously two horizontal components of electric and magnetic fields as E_x, E_y, H_x and H_y. The relation between electric and magnetic fields in horizontal components is described on the Cartesian coordinates as

$$\begin{pmatrix} E_x \\ E_y \end{pmatrix} = \begin{pmatrix} Z_{xx} & Z_{xy} \\ Z_{yx} & Z_{yy} \end{pmatrix} \begin{pmatrix} H_x \\ H_y \end{pmatrix} \tag{5}$$

where Z_{xx}, Z_{xy}, Z_{yx} and Z_{yy} are elements of impedance tensor, Z. Principal axes of impedance tensor as maximum and minimum in perpendicular relation correspond to the elongation of low resistivity zone. When we could assume a two-dimensional structure of low resistivity zone, we could expect the following feature of the direction of maximum axis; (1) parallel to the strike of low resistivity zone at the points on the low resistivity zone, (2) perpendicular at the points near and outside of the low resistivity zone. After the frequency analysis for each component of electric and magnetic fields by FFT (fast Fourier transform) method, and after the transformation to principal axis from the coordinates of measurement to be null impedance of diagonal components of Z in eq. (5), we get principal axis direction of impedance tensor for every frequency of strong ELF-noises. The frequency of ELF-noise relates to the depth of anisotropic structure.

The Yamasaki fault system is traced westward to Toyonari in the Ohara area, Okayama Prefecture, with some bending of strike (Fig. 1 and Fig. 9) (FUKUI, 1981). The strikes of faults in Chugoku district, at the west of the Ohara area, are dominant in N-S sense (R.G.A.F., 1980). The major boundary of the crustal structure should exist in the transition region of fault strikes. The micro-seismicity, furthermore, is linearly concentrated on the zone (called seismic alignment) from Tottori to the

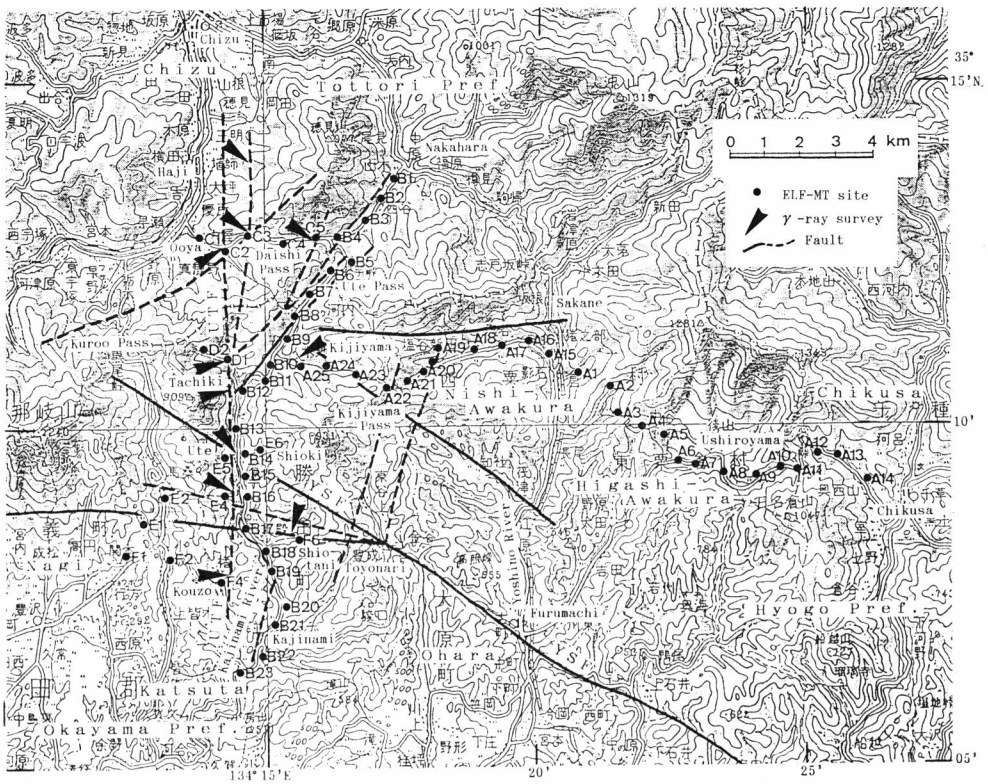

Fig. 9. Location of survey sites and faults in Ohara and Ute areas (after KATSURA *et al.*, 1989). Broken lines are the estimated segments of faults. YSF: Yamasaki fault, UTF: Ute fault.

SSW direction around the transition region (OIKE, 1976). The geological and geophysical surveys are focused on the discovery of fracture zones in this region (KATSURA *et al.*, 1989).

The surveyed area is shown in Fig. 9. Here, the ELF-MT soundings were carried out to find the principal axis directions of impedance tensor. The principal axes of impedance tensor as maximum and minimum are plotted on the map by the apparent resistivity unit as shown in Fig. 10. The unit conversion from impedance to apparent resistivity is based on the eq. (1). Then, the figure (Fig. 10) shows the anisotropic feature of apparent resistivity with respect to the frequency of magnetic and electric fields.

The results suggest that the trend of low resistivity zone would exist in N-S direction along the western side of the Kajinami River, especially from the site B12 to B17. This zone seems to continue to the seismic alignment from Tottori to the SSW direction presented in OIKE (1976). The topographic lineament is also seen

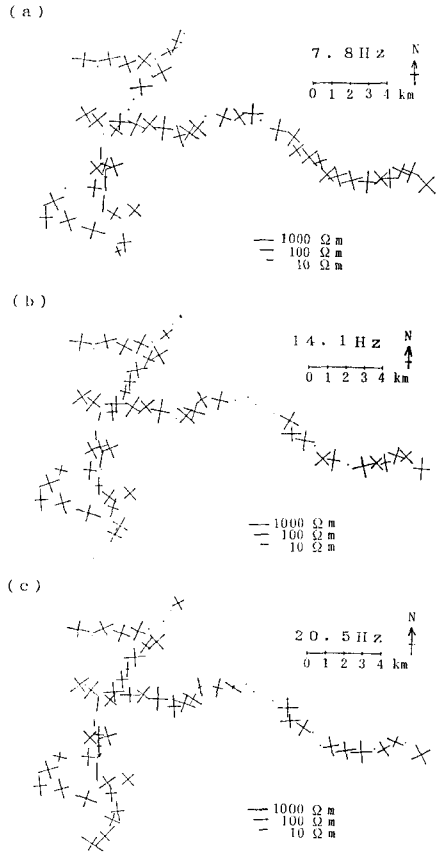

Fig. 10. Principal axis directions of impedance tensor as maximum and minimum in Ohara and Ute areas (after KATSURA *et al.*, 1989). Skewness is less than 0.5. The length of axis is in apparent resistivity unit. ELF-MT sites are shown in Fig. 9. (a) 7.8 Hz, (b) 14.1 Hz and (c) 20.5 Hz.

in this direction. The outcrops of faults were, however, not sufficiently exposed at Ute area. Further analysis of ELF-MT survey as resistivity structure and the γ-ray survey are presented in the later section and in elsewhere (KATSURA *et al.*, 1989).

2.4. Gravity Method

The gravity survey was carried out in two regions; one is in and around Lake Biwa and the other is in the northern part of Ikoma (Fig. 1). This method is suitable for finding a vertical displacement of basement in a wide scale.

Procedure of the gravity survey was the loop method by using spring-type gravimeters. The gravity stations were distributed in uniform spacing about 1 km or

more on the plain. Altitude of the station was determined by the first- or second-order leveling with referring to the bench mark of Geographical Survey Institute (G.S.I.) of Japan. The reference point of gravity is the National Fundamental Gravity Station (F.S.) at Kyoto University. The gravity value at F.S. is 979707.27 mgal on the International Gravity Standardization Net 1971 (IGSN71) (G.S.I., 1976). The gravimeters used were a Worden gravimeter (No. 127) and two LaCoste & Romberg gravimeters (D-36, G-576). The gravity on the lake bottom was measured by a North American gravimeter (RW-160) (ABE and SASAJIMA, 1974). After the tidal and drift corrections, the gravity value is determined from the gravity of reference point. Bouguer anomaly is calculated with assuming of mean crustal density after the atmospheric correction, free-air reduction and terrain correction. Terrain correction is performed to circular area of 50 km radius for a gravity station with taking account of curvature of earth's surface (KATSURA *et al.*, 1987b). The meshed digital map of topography KS-110-1 published by G.S.I. is used in the terrain correction.

Underground structure is estimated from distribution of Bouguer anomaly values. Densely parallel contours of isogals in the Bouguer anomaly map suggest vertical displacement of basement after folding and faulting. Two-dimensional model is effective to this case. The inversion method is based on the manner of TALWANI *et al.* (1959) with parameters of layer boundary and density difference between sediments and basement. When we could obtain the data of basement depth after well drilling, we refer to the data as the reference level at the drilling site for the computer fitting of the inversion.

The widest region surveyed by the gravity method is in Shiga Prefecture, in and around Lake Biwa, northeastern part of Kinki district (Fig. 1) (NISHIDA *et al.*, 1990). Lake Biwa is the largest lake of Japan and the thick sediment layers are deposited in its basin (HORIE and TANAKA, 1983). The source data partly includes lake bottom gravity measured by ABE and SASAJIMA (1974) and two graduate theses of Kyoto University (NOGUCHI, 1976; SUDA, 1981). The data processing to calculate Bouguer anomalies is described in KATSURA *et al.* (1987b). Bouguer anomaly map is shown in Fig. 11.

Fig. 11 also shows faults inferred from the isogal contour pattern. The estimated faults shown in the figure enclose the outside of lake basin and gather along the boundary between mountainous region and plain. Some of the estimated faults coincide with the faults recognized by the geological studies (TOGO, 1971, 1974; MURAI and KANEKO, 1975; R.G.A.F., 1980). The examples are shown in the Yanagase, the Hanaori, the Hiei, the Hira, the Katata, the Sanami, the Makino, the Aibano, the Suzuka (Hyakusaiji) and the Tongu faults.

Subsurface structure is modeled by the two layers composed of sedimentary

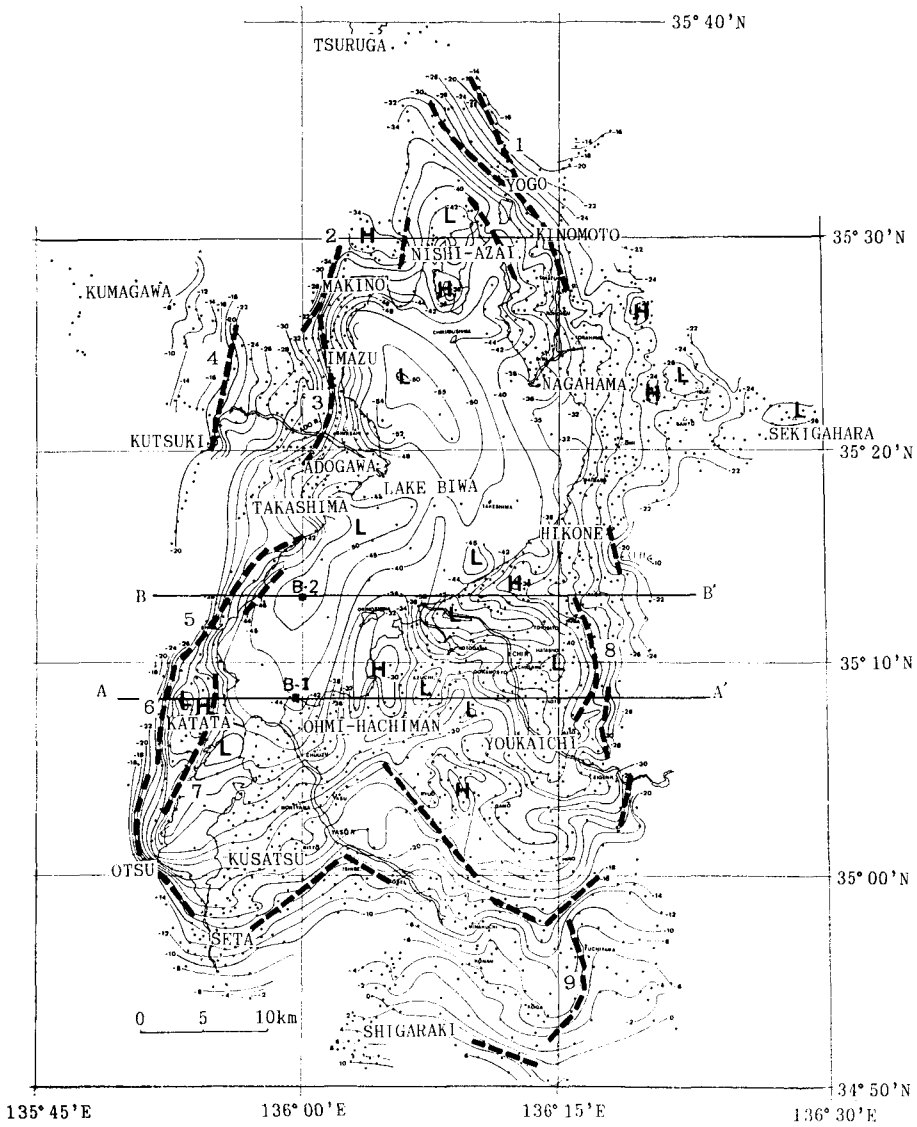

Fig. 11. Bouguer anomaly map in and around Lake Biwa (modified from NISHIDA *et al.*, 1990). Solid circle is gravity station. Contour interval is 2 mgal on land and 5 mgal in the lake. Assumed Bouguer density is 2.4 g/cm^3. H and L are maximum and minimum centers of anomaly, respectively. Bold dashed lines are faults inferred from dense isogal contours of Bouguer anomaly. 1: Yanagase fault, 2: Sanami fault, 3: Aibano fault, 4: Hanaori fault, 5: Hira fault, 6: Hiei fault, 7: Katata fault, 8: Suzuka (Hyakusaiji) fault, 9: Tongu fault. B-1 and B-2 are drilling sites to reach basement.

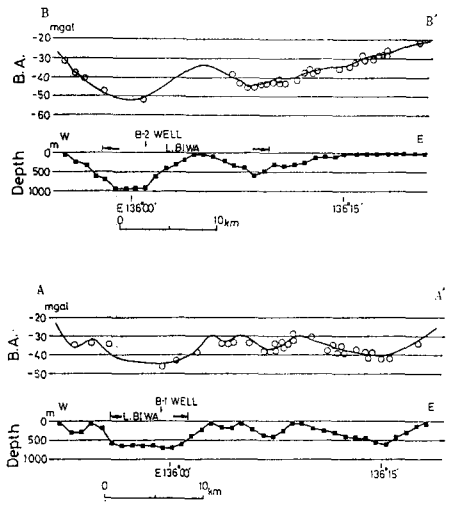

Fig. 12. E-W section along the lines A-A' and B-B' shown in Fig. 11 (after NISHIDA *et al.*, 1990). B.A. is Bouguer anomaly shown by isogal contours (solid line) and by projections of Bouguer anomaly values at the gravity stations inside the belt zone of 1 km wide from the lines (open circle). Depth is of basement relative to the water level of Lake Biwa at 85 m of altitude. B-1 and B-2 drilling positions are fixed points of basement level in the process of two-dimensional analysis. Assumed density difference between sediments and basement is 0.6 g/cm^3.

layer and basement. Fig. 12 shows two examples of basin structure in E-W sections. The figure suggests the existence of the folding and the Hira and the Suzuka faults. There is also some effects of the Katata fault on A-A' section and the fault along west coast of the lake on B-B' section. A remarkable feature is rhyolite body in the Koto plain near Ohmi-Hachiman at the center of A-A' section.

Implication of the sections concerning to folding and faulting is that the Hira-Hiei and the Suzuka mountains relatively uplifted to the lake basin. The vertical faulting at the west side is more vigorous than that at the east side. Further analysis is presented in elsewhere (NISHIDA *et al.*, 1990).

Another gravity survey was carried out at the Takayama area, in the northern part of Ikoma City, Nara Prefecture (Fig. 1). The surveyed area is a small sedimentary basin surrounded by granitic basement. In and around this area, many active faults run in a complicated manner (Fig. 13). And, the north-south striking faults are considered to be vertical-slip (reverse) type (*e.g.* R.G.A.F., 1980).

The gravity stations were arranged to be about 200 m to 300 m mesh. Bouguer anomaly values were calculated by the manner of KATSURA *et al.* (1987b). Bouguer anomaly map (Fig. 13) shows a linear trend of parallel dense isogal contours with N10°E strike parallel to the Tomio River at the central part. The east side of basement has relatively uplifted. This trend agrees with the trace of the Miyakata fault

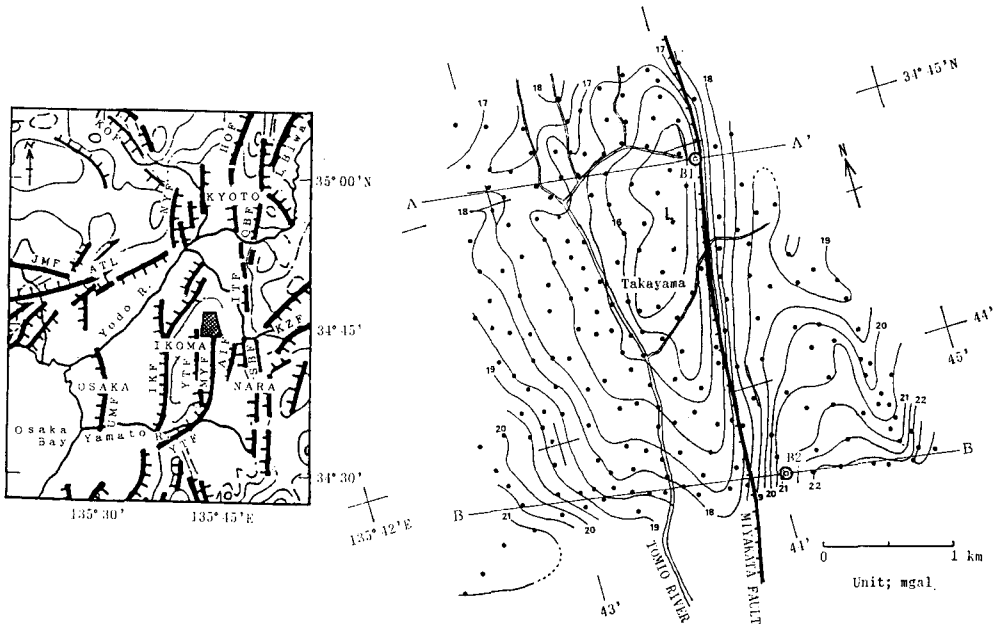

Fig. 13. Bouguer anomaly map in Takayama area, northern part of Ikoma City, Nara Prefecture. Solid circle is gravity station. Contour interval is 0.5 mgal. Assumed Bouguer density is 2.67 g/cm^3. B1 and B2 are drilling sites to reach granitic basement. IKF: Ikoma fault, YTF: Yata fault, MYF: Miyakata fault (or Tomiogawa flexure), AIF: Ayameike flexure, SBF: Sabota flexures, KZF: Kizugawa fault, ITF: Ite fault, OBF: Obaku fault, HOF: Hanaori fault, NYF: Nishiyama fault, KOF: Kameoka fault, ATL: Arima-Takatsuki tectonic line, JMF: Jumantsuji fault, UMF: Uemachi fault, YTF: Yamatogawa fault.

(or the Tomiogawa flexure in R.G.A.F., 1980). This fault is parallel to the Ikoma and the Yata faults (Fig. 13). The deepest point of sedimentary basin is located in the western side of this fault.

The underground structure was analyzed by the two-dimensional Talwani method (TALWANI *et al.*, 1959). In this process, we employed the known levels of basement at the two drilling sites. Two sections across the fault are shown in Fig. 14. The fault structure and the shape of sedimentary basin are clear estimated. The vertical-slip of the Miyakata fault is more than 200 m. This estimation implies that the Miyakata fault is one of the N-S striking major faults. Tectonic significance of this fault will be discussed later.

3. Active Faults in Hidden and Uncertain Areas

The surveyed areas in the course of this study are shown in Fig. 1. Most of

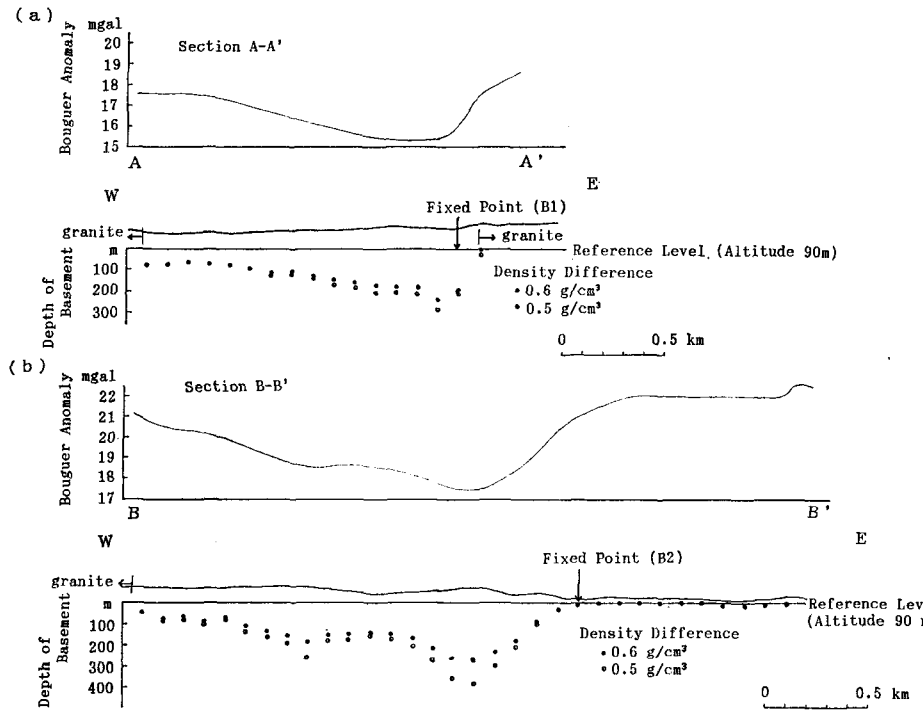

Fig. 14. Sections along A-A' (a) and B-B' (b) lines shown in Fig. 13. Density difference between basement and sediments is assumed to be 0.6 and 0.5 g/cm^3. Reference level of subsurface structure is at 90 m of altitude. Sections of A-A' and B-B' are referred to two known levels of basement rock (granite) at the drilling sites.

these areas were not catalogued as the places of faulting before this study (R.G.A.F., 1980), but some places had already been recognized as the active faults. For the latter, the techniques of prospecting active fault were tested. The results of surveys except the above-mentioned examples are presented in the followings:

3.1. East Extension of the Yamasaki Fault

The Yamasaki fault is a typical left-lateral strike-slip active fault in the northwestern part of Kinki district (Fig. 1) (HUZITA, 1969). The Yamasaki fault shows active micro-seismicity and the activity of the fault is monitored for earthquake prediction by some geophysical and geochemical methods (KISHIMOTO, 1981). The Yamasaki fault system is composed of several faults and situated at the topographic boundary between the northern mountainous area and the southern hilly area. The continuation of Yamasaki fault system has been confirmed to be about 80 km with WNW to ESE striking (FUKUI, 1981). The southeastern end around Fukusaki is the obscured area for the location of fault lines. The epicenters of micro-earthquakes,

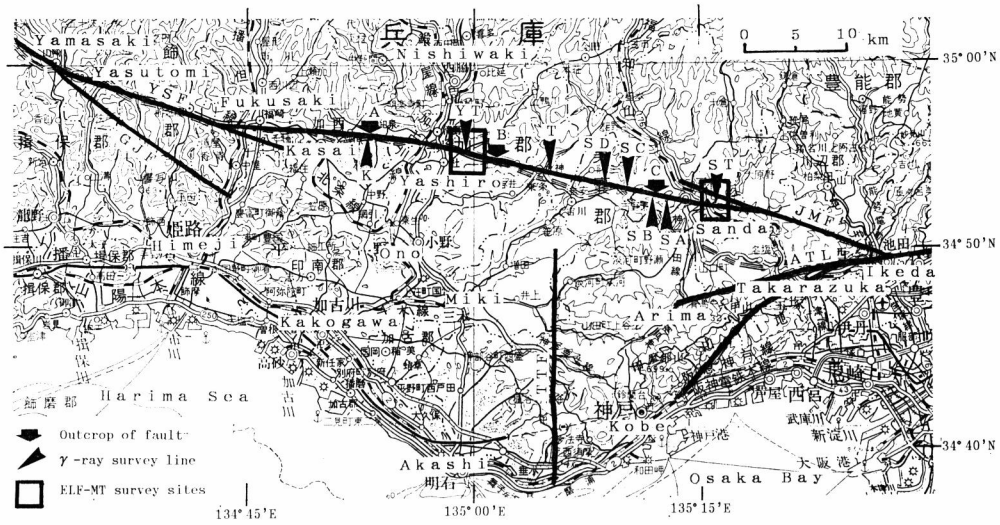

Fig. 15. Location of survey sites and faults in the area between Fukusaki and Sanda (after Mogi *et al.*, 1985a). YSF: Yamasaki fault, GJF: Goji fault, JMF: Jumantsuji fault, ATL: Arima-Takatsuki Tectonic Line, TTF: Takatsukayama fault.

however, are distributed in a straight array extending to the Jumantsuji fault, a branch of ATL, from the Yamasaki fault (Oike, 1976). This fact suggests the existence of a hidden active fault connecting the Yamasaki and the Jumantsuji faults.

The geological and geophysical surveys were carried out in this area (Fig. 15) (Mogi *et al.*, 1985a). In Fig. 15, the line between Fukusaki and Sanda through Kasai and Yashiro is the newly discovered active fault called the Yashiro fault. The long chain of the Yamasaki and the Yashiro faults make a major active fault system called the Sanda-Yamasaki tectonic line (STL). The fault outcrops show the strike of N50°W to N70°W and the dip of 60°S to 70°S. There are many hot and cold springs along the STL including the Yamasaki fault and the ATL (Koizumi *et al.*, 1986). Although the utilization of springs is controlled by the economic purpose, the linear distribution of springs supports the existence of hidden active faults.

The ELF-MT soundings were carried out along two survey lines across the hidden STL (Fig. 15). The results are shown in Fig. 16 for the Yashiro line and in Fig. 17 for the Sanda line. The TM-mode profiles of apparent resistivity shown in both (b) of Fig. 16 and Fig. 17 are the case that the magnetic field is in E-W direction. These profiles suggest the location of fault line and fracture zone. In the Yashiro area, the fault runs between the sites D and E, and the fracture zone is considered to spread to the site I. In the Sanda area, fractures are located near the sites C and E.

The one-dimensional analysis was performed and the solutions were given in Mogi *et al.* (1985a). After this process, the location of fault line and the size of

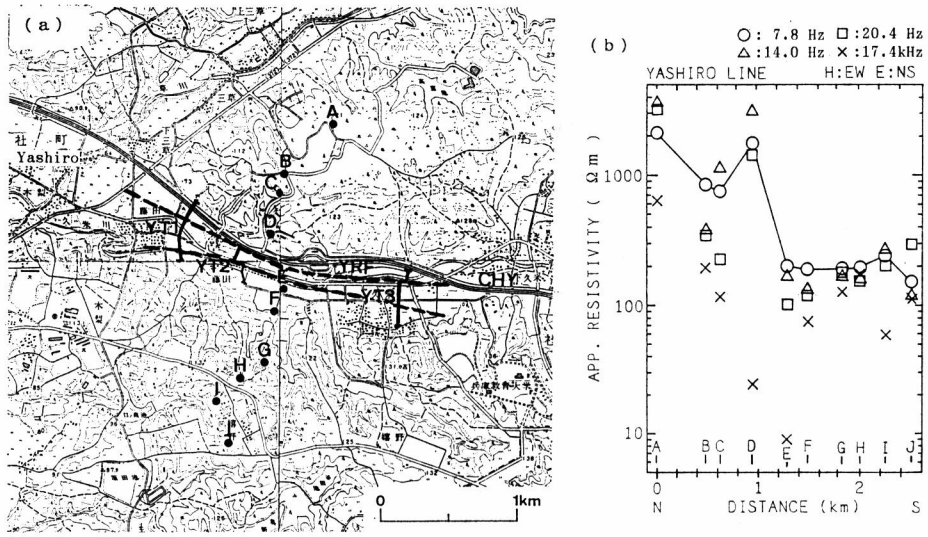

Fig. 16. ELF-MT soundings at the Yashiro area (after MOGI *et al.*, 1985a). (a) Location of ELF-MT (solid circle) and the γ-ray (solid line) survey sites. YRF: Yahsiro fault as a part of Sanda-Yamasaki tectonic line (STL), CHY: Chugoku Highway. (b) N-S apparent resistivity profile (TM-mode).

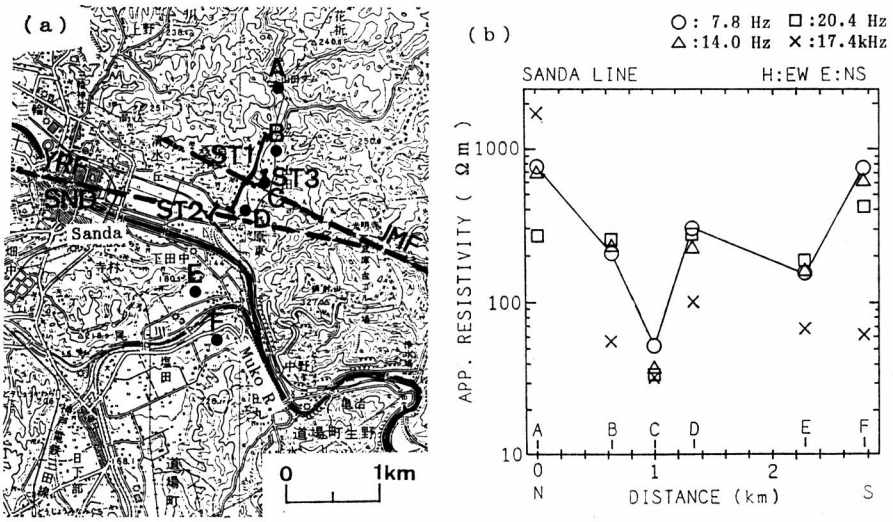

Fig. 17. ELF-MT soundings at the Sanda area (after MOGI *et al.*, 1985a). (a) Location of ELF-MT (solid circle) and the γ-ray (solid line) survey sites. SND: Sanda, JMF: Jumantsuji fault, YRF: Yashiro fault as a part of STL. (b) N-S apparent resistivity profile (TM-mode).

fracture zone could be reliably estimated. The preliminary estimations of fault line and fracture zone on the apparent resistivity profiles are confirmed. The fracture zones at the Yashiro and Sanda areas are more than 1.5 km of width.

The typical results of γ-ray survey across the STL are shown in Fig. 18. The peak points of γ-ray intensity almost agree with the fault positions estimated from the ELF-MT results (see Fig. 16 and Fig. 17). At the end of surveys, we could estimate the trace of hidden active fault by combining the results of ELF-MT and γ-ray with the geological and topographical features. The estimated fault lines shown in Fig. 15, Fig. 16(a) and Fig. 17(a) are the results after this process.

The displacement of Yamasaki fault is left-lateral in the Yasutomi area, the main part of the present Yamasaki fault (FUKUI, 1981). The displacement of Jumantsuji fault is also left-lateral (HUZITA *et al.*, 1971). The Yamasaki fault at Yasutomi was evaluated to have a fractured zone with a width of about 2 km (E.R.G.A.F., 1982) or about 6 km (HANDA and SUMITOMO, 1985). Combining these results with the results mentioned above, we can estimate that the STL is a long active fault system with wide fracture zone, about 2 km or more of width, and the left-lateral displacement.

The Yamasaki fault system has the displacement with left-lateral strike-slip

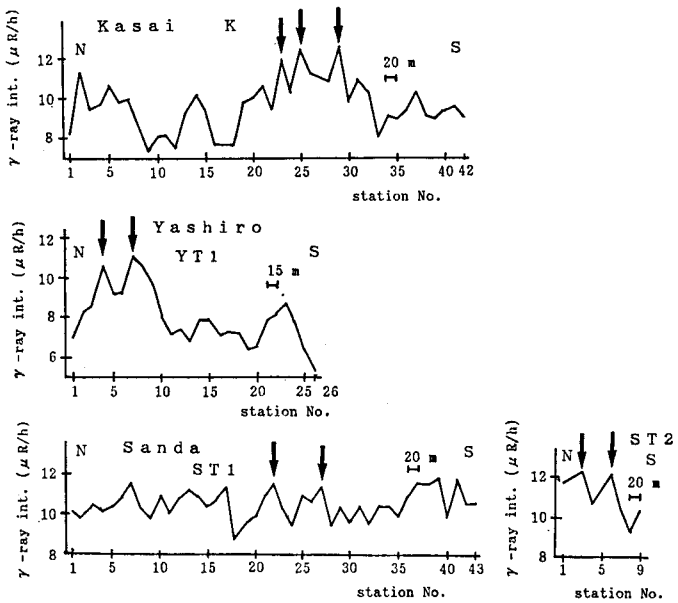

Fig. 18. Examples of γ-ray profiles at the surveyed lines across the Sanda-Yamasaki tectonic line (after MOGI *et al.*, 1985a). Arrows show the possible positions of fault planes at surface. K, YT1 and ST are the N-S survey lines at the Kasai, Yashiro and Sanda areas, respectively, as shown in Fig. 15, Fig. 16(a) and Fig. 17(a).

associated with the uplift of the northern massif (FUKUI, 1981). The uplift is severe at the northern massif than the southern massif in the whole parts of STL. The ATL system, which is linked from the STL system through the Jumantsuji fault, has also the same sense of vertical displacement, but has a right-lateral strike-slip (SANGAWA, 1978; HUZITA and KASAMA, 1982). Though there is a difference in the strike-slip sense, the STL and the ATL systems make a tectonic boundary between the northern mountainous area and the southern hilly or plain area. The northern area corresponds to the region dominated by Mesozoic and Paleozoic sedimentary rocks and partly covered by late Mesozoic effusives (HUZITA, 1974). On the contrary, the southern area is widely covered by thick alluvium and terrace formations with some late Mesozoic effusives and granitic rocks.

3.2. Western Border of the Yamasaki Fault

The Yamasaki fault system is traced westward to Toyonari, in the Ohara area, Okayama Prefecture (Fig. 1) (FUKUI, 1981). This area is considered to be the major boundary of the crustal structure between Kinki and Chugoku districts because of the difference of active fault pattern (R.G.A.F., 1980). The surveyed area and the estimated fault pattern are previously shown in Fig. 9.

In this area, the ELF-MT soundings were carried out to find the distribution of principal axis of impedance tensor. The results and preliminary interpretation are presented before (see Fig. 10). Furthermore, the analysis of resistivity structure and the γ-ray survey were also carried out.

The apparent resistivity profiles as scalar resistivity and the resistivity sections by the one-dimensional analysis are shown in Fig. 19. The scalar apparent resistivity was calculated from an orthogonal set of magnetic and electric fields as the amplitudes of FFT spectra. The most remarkable trend of low resistivity zone is recovered in N-S direction through Ute and Kajinami from Chizu. The main structure of low resistivity zone exists in the west side of Kajinami River.

The γ-ray survey was carried out to find the extent of fracture zone at Ute area (Fig. 9). The results are shown in Fig. 20. The high level of γ-ray intensity in the region of Tachiki, northern Ute (Fig. 20(b)), is attributed to the wide exposure of granitic rocks, but some portions are sings of fractures. On the contrary, the high intensity of γ-ray on the E-W survey lines around Shioki (Fig. 20(c)) reflects northwest extension of the Yamasaki fault. The results suggest that the western end of Yamasaki fault spreads branches like spray faults and faces to the N-S fault at Ute.

Main fault structures in this area are concluded to be the two lines shown in Fig. 9. One is named the Ute fault which is newly defined in this study. Another is the west end of Yamasaki fault system which faces to the N-S striking Ute fault with some spreads of branches. The trend of Ute fault agrees with the southern

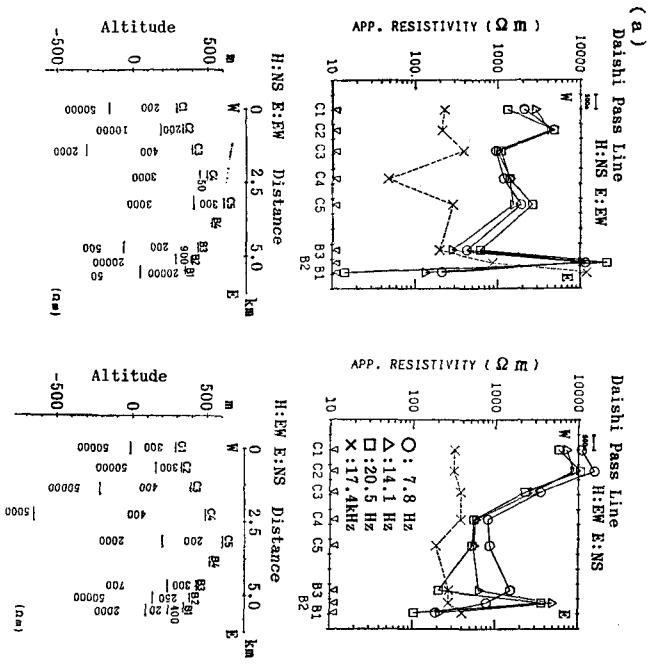

Fig. 19 (a)

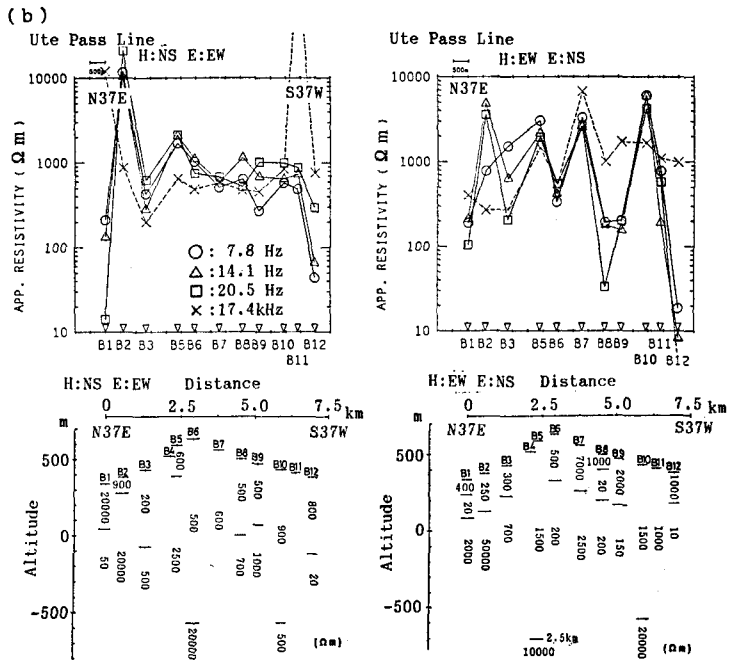

Fig. 19 (b)

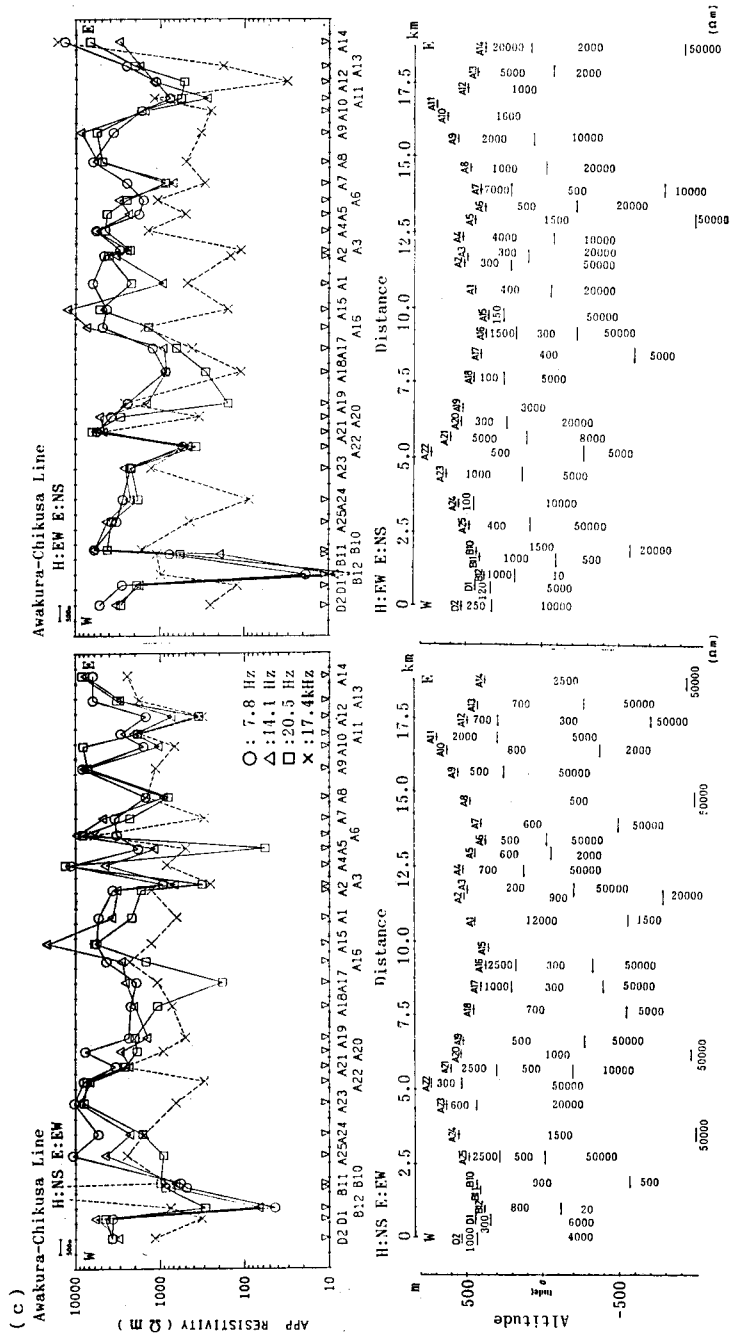
(c)
Awakura-Chikusa Line
H:NS E:EW
H:EW E:NS
Distance
APP RESISTIVITY (Ω m)
Altitude
○ : 7.8 Hz
△ : 14.1 Hz
□ : 20.5 Hz
× : 17.4kHz

Fig. 19 (c)

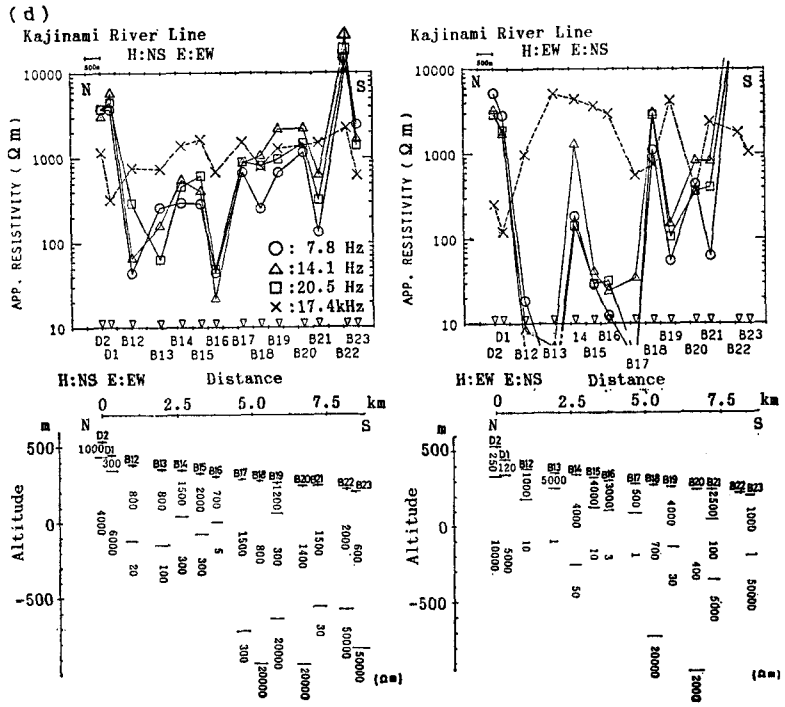

Fig. 19 (d)

Fig. 19. Apparent resistivity profiles and resistivity sections estimated by one-dimensional analysis for Ohara and Ute areas. Surveyed sites are shown in Fig. 9. (a) E-W line at Daishi Pass. (b) NE-SW line from Nakahara to Tachiki through Ute Pass. (c) E-W line from Chikusa to Ute through Awakura and Kijiyama Pass. (d) N-S line along the Kajinami River.

extension of seismic alignment between Tottori and Chizu (OIKE, 1976) and with the lineament of topography. The line of Ute fault can be assumed to be the major boundary dividing the geologic structure between Kinki and Chugoku districts. The tectonic zones in this area were discussed in detail by KATSURA *et al.* (1989).

3.3. Continuity of the Yagi-Yabu Fault and the Mitoke Fault

There is a gap of about 25 km in distance between the Yagi-Yabu fault and the Mitoke fault (Fig. 1). The epicentral distribution of micro-earthquakes, however, makes a chain of seismic alignment between these two faults (OIKE, 1976). This alignment runs through the Yabu-Mitoke area in Yakuno and Fukuchiyama, Kyoto Prefecture. The topographic lineament also shows a possibility of existence of active fault. The surveyed area was chosen in Yakuno and Fukuchiyama (Fig. 21) and the geological and geophysical surveys were performed (MOGI *et al.*, 1985b).

The geological survey was first carried out to find the fault outcrops and springs.

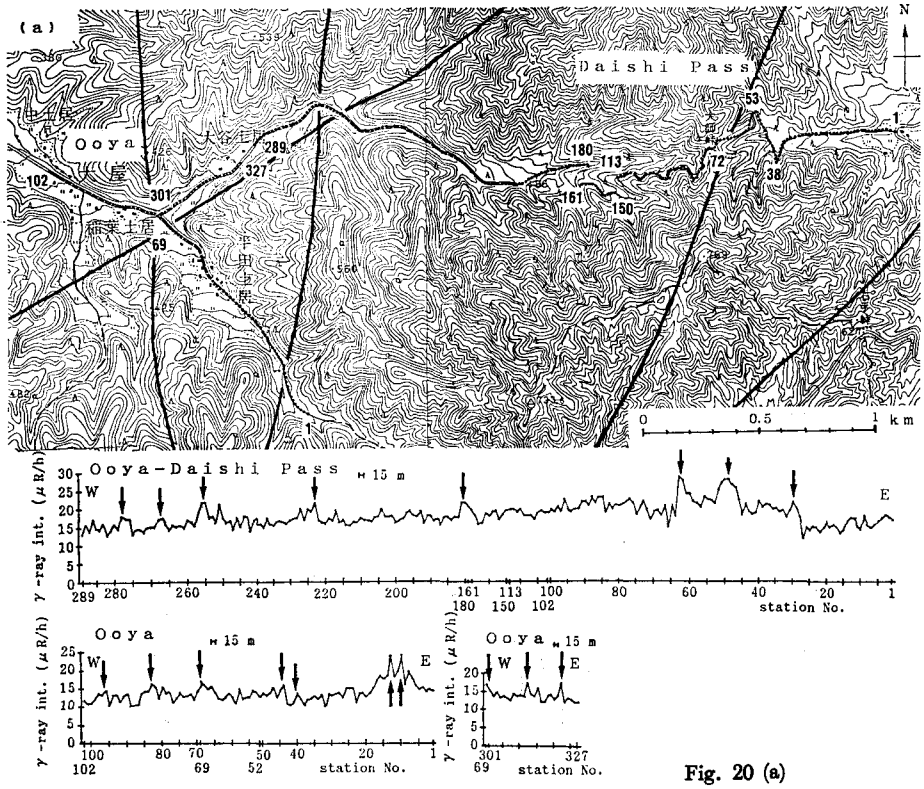

Fig. 20 (a)

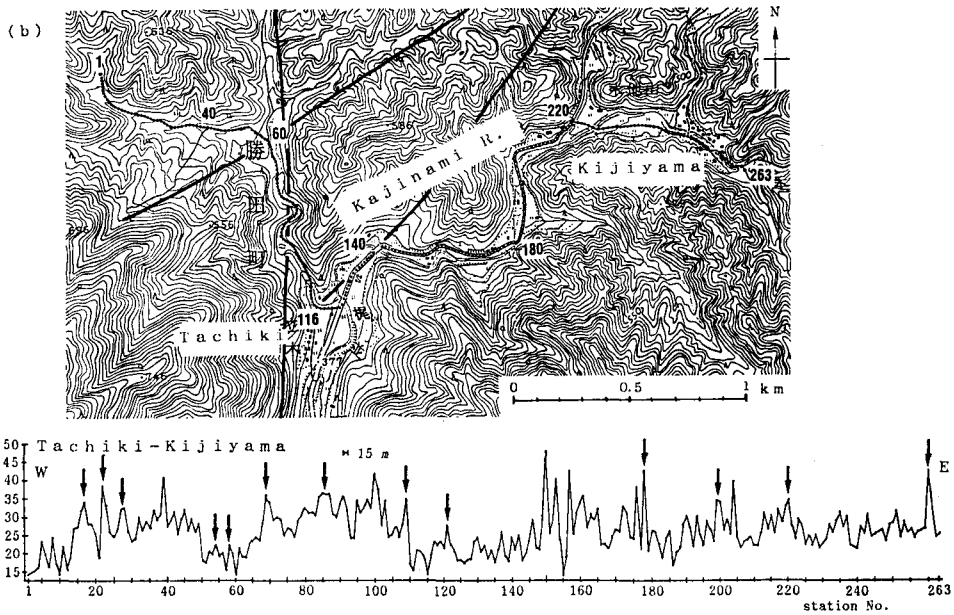

Fig. 20 (b)

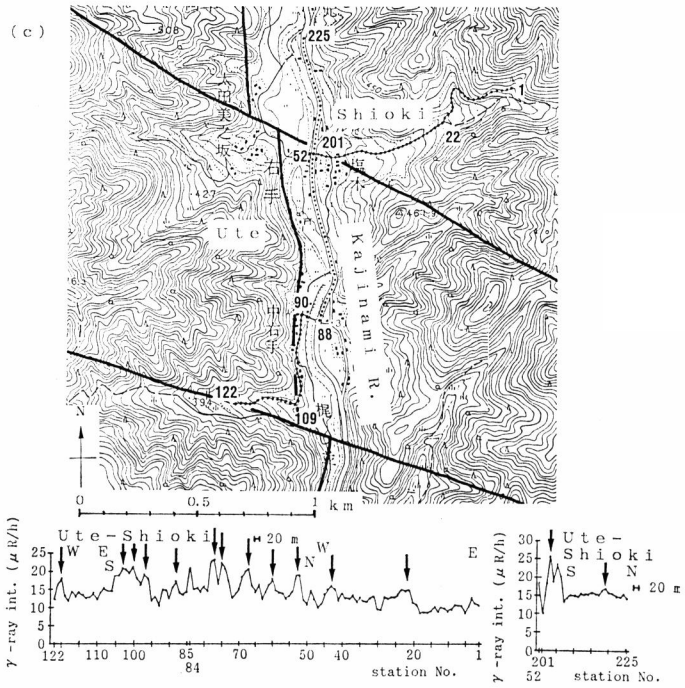

Fig. 20 (c)

Fig. 20. Examples of γ-ray profiles and site maps at Ute area (after KATSURA *et al.*, 1989). Arrows show the possible positions of fault plane at surface. Fault lines (solid line) are inferred from ELF-MT and γ-ray surveys with topographic lineaments. (a) E-W line at Daishi Pass. (b) E-W line from Tachiki to Kijiyama. (c) Lines at Shioki.

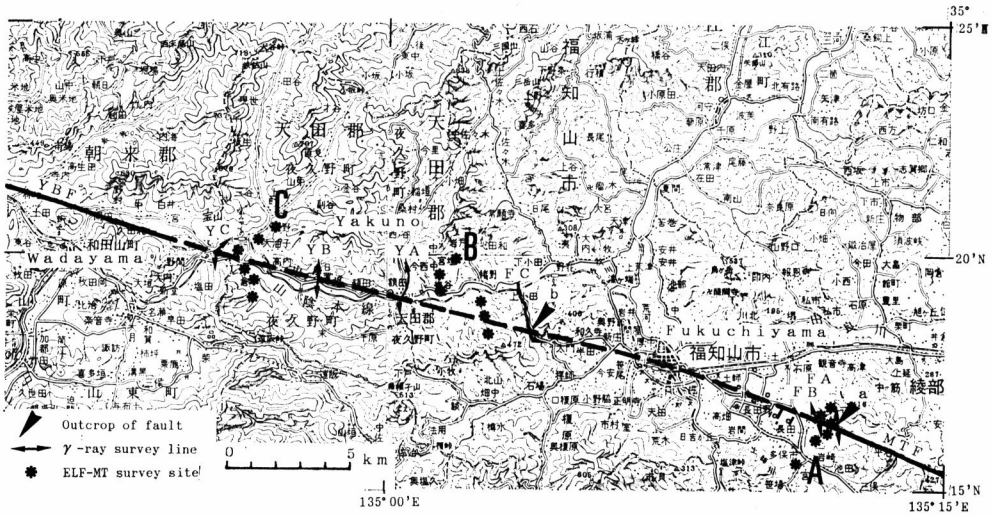

Fig. 21. Location of survey sites in Fukuchiyama and Yakuno areas (after MOGI *et al.*, 1985b). MTF: Mitoke fault, YBF: Yabu fault. Dashed line is the estimated portion of the fault.

The surveyed area is mainly exposed by Permian to Triassic Maizuru and Yakuno groups comprising sedimentary rocks and of Yakuno complex mainly composed of gabbro. The terrace deposits unconformably cover those old layers around Fukuchiyama. The outcrops of fault (Fig. 21) reveal the slip in the old rocks, but the faulting in younger layer is not clear. The strike of faults, in any case, is concordant with WNW-ESE direction of the lineament.

The γ-ray survey and the ELF-MT soundings were carried out at several lines across the lineament (Fig. 21). The results of γ-ray survey shown in Fig. 22 indicate the consistency between the fault outcrops and the peak points of intensity, especially in the FC line.

The apparent resistivity profiles shown in Fig. 23 do not reveal a remarkable feature of low resistivity zone, but there is only a sign of low resistivity zone at the northern part of the line A (Fig. 23(a)) on east of Fukuchiyama. The one-dimensional models of resistivity structure estimated by MOGI *et al.* (1985b) suggest that there is also a remarkable fracture zone at the northern part of the line A. The low resistivity zone, however, is not clearly detected in the underground structure at the west of Fukuchiyama and at Yakuno.

As the surveyed lines were across the lineament as the expected trace of the fault, the absence of remarkable low resistivity zone implies the following two reasons. The first is that there is a minor fracture zone which could not be detected by the

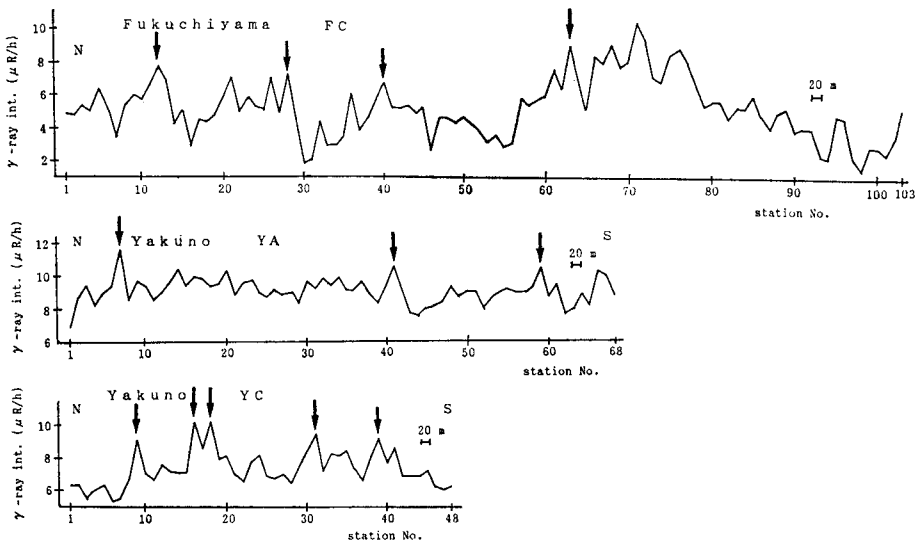

Fig. 22. Examples of N-S γ-ray profiles at Fukuchiyama and Yakuno areas (after MOGI *et al.*, 1985b). Arrows show the possible positions of fault plane at surface. Line name corresponds to Fig. 21.

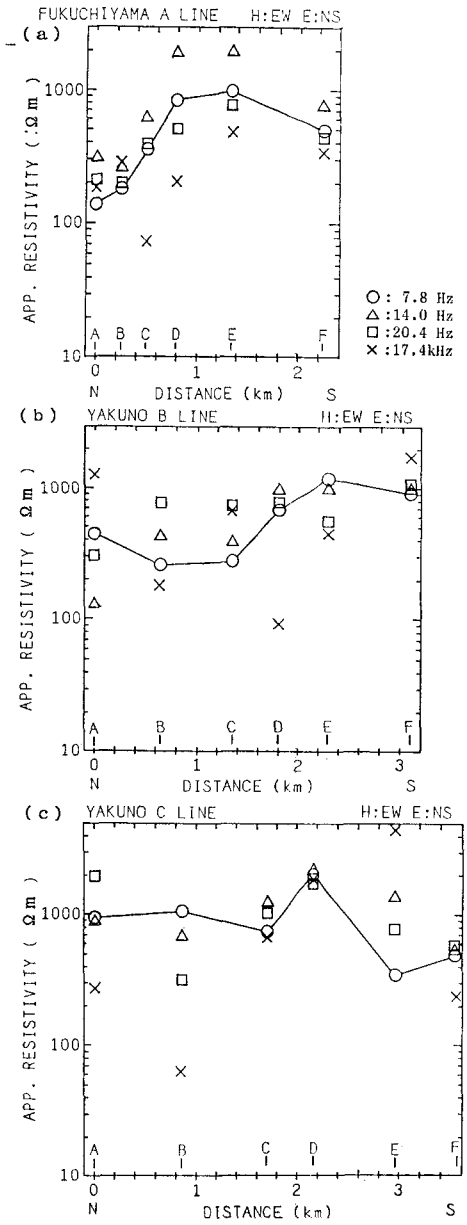

Fig. 23. N-S apparent resistivity profiles of ELF-MT soundings at Fukuchiyama and Yakuno areas (after Mogi *et al.*, 1985b). Surveyed sites are shown in Fig. 21.

ELF-MT sounding. The second is that the fault is inactive at present after the last stage of faulting and that the fracture zone has not low resistivity. The fault which has an old age of last faulting loses the feature of low resistivity at the fracture (E.R. G.A.F., 1982). This is explained by the concretion mechanism of fracture zone after the interruption of fluid water. In fact, the Yabu fault is considered to have the age of last faulting before middle Pleistocene (R.G.A.F., 1980).

The fault between the Yabu and Mitoke faults is estimated by the results mentioned above. We call the fault in this portion as the Fukuchiyama fault. The resistivity structure at the east of Fukuchiyama and the γ-ray intensity profiles suggest the width of fracture zone as about 1 km or more. The fault includes many minor faults as echelons. The fault system is, therefore, composed of the Mitoke, Fukuchiyama, Yabu and Yagi faults. The extension of this fault system is beyond 100 km from the northwest of Kyoto to Sekinomiya with strike of N70°W to N80°W. This fault system is mainly left-lateral strike-slip and the south side is relatively uplifted. Some parts of the Mitoke fault, however, show right-lateral motion (R.G. A.F., 1980).

3.4. The Yagi Fault

The Yagi fault is a geologic boundary having an E-W strike between the Hokutan group and the serpentinite body (WADATSUMI and MATSUMOTO, 1958). The trace of fault shows a length of about 20 km (Fig. 1) (R.G.A.F., 1980). The survey on this fault was carried out at Sekinomiya, Hyogo Prefecture (KATSURA *et al.*, 1987a). The results were presented before: The geological survey and the estimated traces are shown in Fig. 2, the γ-ray profiles in Fig. 5, the apparent resistivity profiles in Fig. 7, and the resistivity sections in Fig. 8. The fracture zone is clear at the Miyake area and the estimated dimension is about 300 m of width and 900 m of depth.

The Yagi fault has a wide and deep fracture zone, and there is scarce occurrence of micro-earthquakes along the fault. This anomalous relation suggests two possibilities. The first is that the Yagi fault is in a rest period of its activity and fills only the role of a major boundary of geologic provinces. The second is that there is a mechanism of release of stress in the serpentinite body.

The Yagi fault is traced westward to the mountain foot of Mt. Hyonosen into Pleistocene volcanics (Fig. 2). In the farther west of Mt. Hyonosen, the fault disappears. The seismic alignment with N-S direction from Tottori to the west-end of Yamasaki fault (OIKE, 1976) seems an active fault bounding the west-extension of Yagi fault which is supposed. On the contrary, the east-end of the Yagi fault is traced to encounter the Yabu fault with some bend as about 20° at the west of Yoka. The Yagi and Yabu faults make a continuous fault system called the Yagi-Yabu fault.

Furthermore, the southwest extension of Yamada fault falls in the conjunction point of Yagi and Yabu faults (Fig. 1) (NISHIMURA *et al.*, 1986).

3.5. Southwest Extension of the Yamada Fault

The Yamada fault was associated with the *M*7.3 Kita-Tango earthquake (*M* means magnitude) which occurred at March 7, 1927, around the epicenter of 135° 09'E, 35°32'N (JAPAN METEOROLOGICAL AGENCY [hereafter called J.M.A.], 1982). The displacements of the ENE-WSW striking Yamada fault and the NNW-SSE striking Gomura fault have occurred as a conjugate system at the Kita-Tango earthquake (Fig. 1). The displacement of Yamada fault is right-lateral strike-slip and the southeast side relatively depressed. The trace of Yamada fault is only confirmed about 8 km of length at the base of Tango Peninsula from Iwataki to Nodagawa (Fig. 24). The southwest extension of Yamada fault was considered to be the Nakafuji fault as a bending part from west-end of the Yamada fault (UEMURA, 1985).

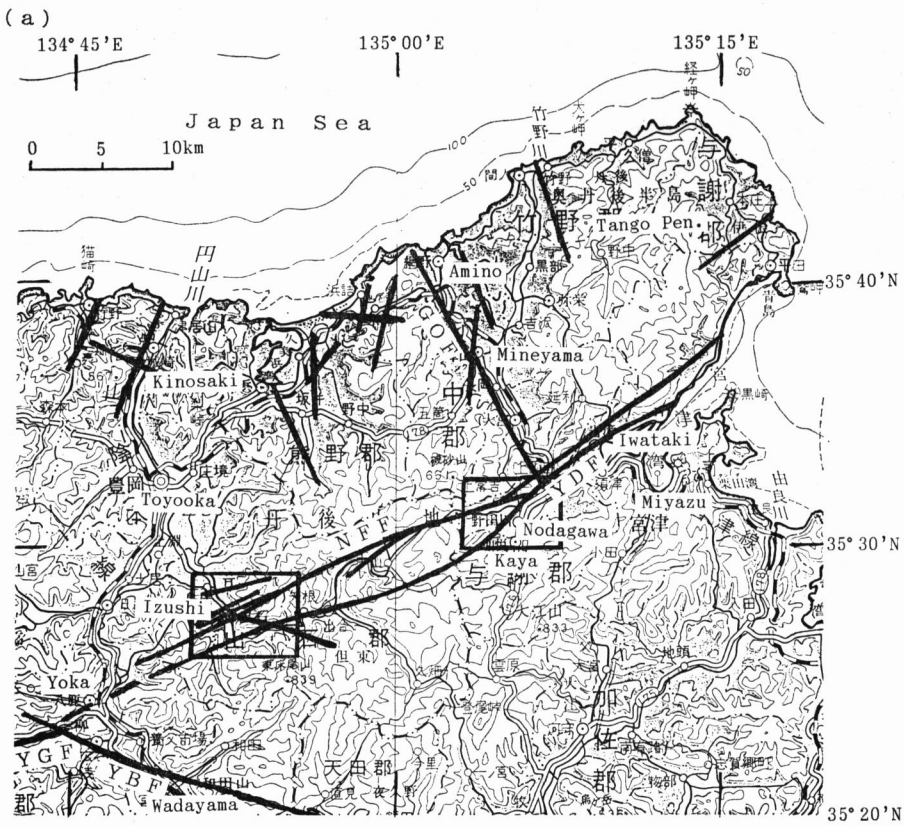

Fig. 24 (a)

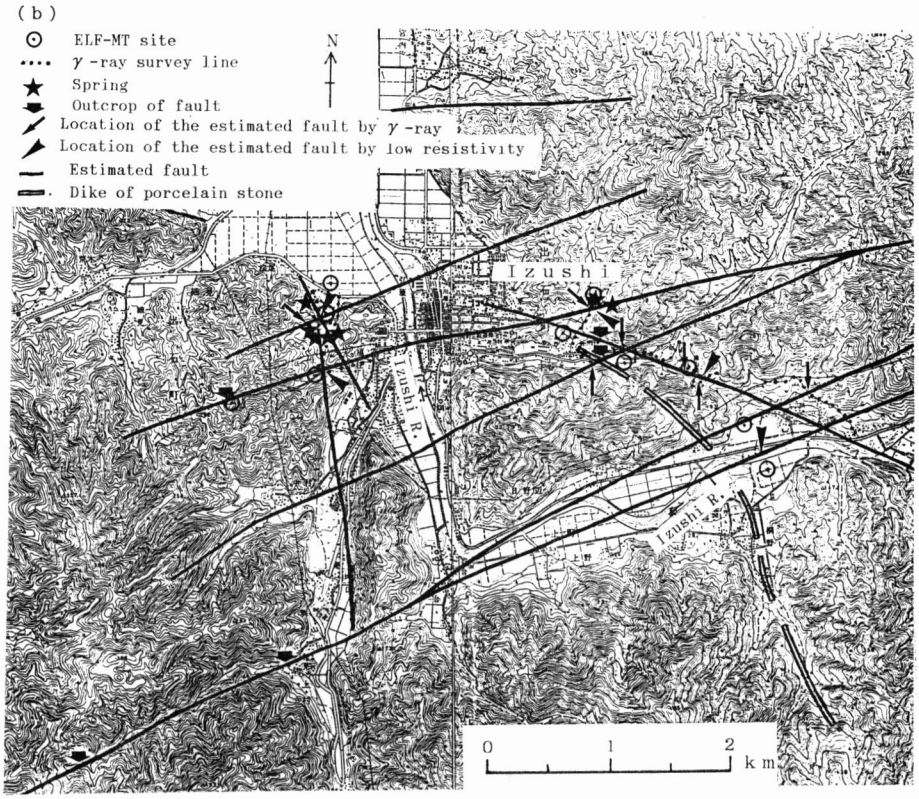

Fig. 24 (b)

In the areas of the southwestern end of Yamada fault, we conducted geological and geophysical surveys to find a sign of fault trace at Izushi, Hyogo Prefecture, and Nodagawa, Kyoto Prefecture (Fig. 1). The surveyed areas are shown in Fig. 24. The geological survey was performed to find out the fault outcrops and the distribution of artesian springs. The geophysical surveys were based on the ELF-MT and the radioactive methods. Parts of the results are shown in Fig. 25 for the γ-ray surveys and in Fig. 26 for the ELF-MT soundings. Details of the results are presented in NISHIMURA *et al.* (1986) for the Izushi area and in KATSURA *et al.* (1987a) for the Nodagawa area.

The apparent resistivity profiles reveal the existence of a fracture zone, but at Nodagawa (Fig. 26(a)) the profiles show obscure results. The mode separation between TM and TE was not successful. The one-dimensional analysis was applied to the measured results for both Izushi and Nodagawa. The resistivity model of Izushi suggests that two deep fracture zones with parallel relation in separating about 2 km run through in ENE-WSW direction (NISHIMURA *et al.*, 1986). The resistivity

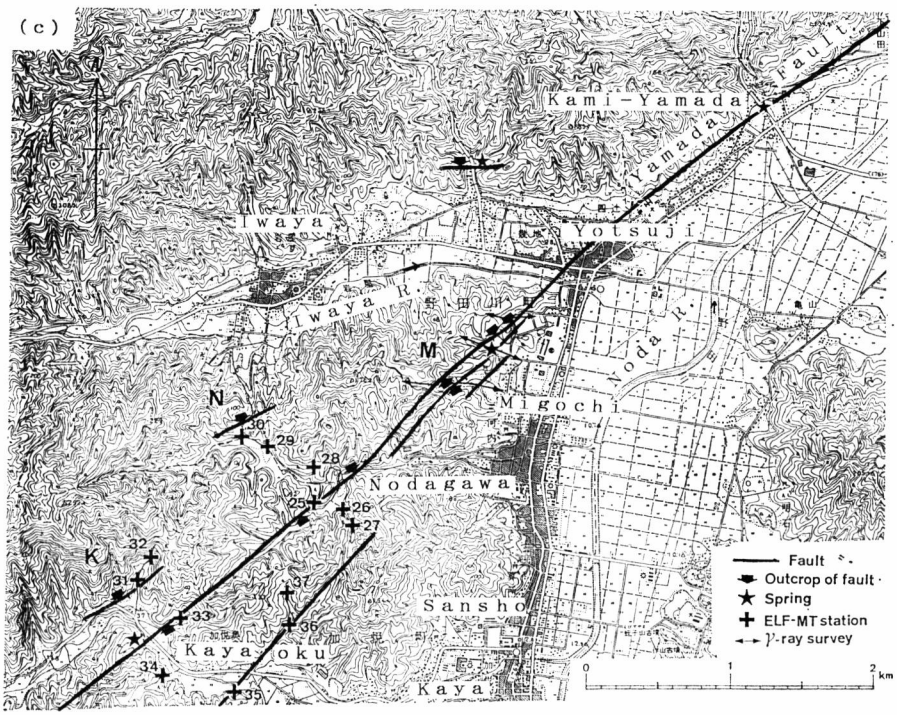

Fig. 24 (c)

Fig. 24. Location of survey sites for the southwest extension of Yamada fault. (a) Index map showing fault structures. YDF: Yamada fault, GOF: Gomura fault, NFF: Nakafuji fault, YBF: Yabu fault, YGF: Yagi fault. (b) Izushi area (after NISHIMURA *et al.*, 1986). (c) Nodagawa area (after KATSURA *et al.*, 1987a).

structure of Nodagawa indicates that the fracture zone with relatively shallow as about 500 m of depth is extended for the whole range of surveyed lines (Fig. 27). According to the evidences of lineament, fault outcrops, γ-ray peaks and resistivity models, the fracture zone stretches from the southwest end of Yamada fault at Yotsuji, Nodagawa-Cho, to the west-southwest direction with about 2 km of width. The north border of this fracture zone is considered to be the Nakafuji fault. In fact, the minor faults as echelons are developed in this estimated fracture zone with E-W strikes. The terminal of southwest extension of this fracture zone should arrive at the conjunction point of the Yagi and Yabu faults.

The dimensions of fracture zone is relatively wide. The micro-seismicity along the Yamada fault and the southwest extension is not so high. On the contrary, the Gomura fault, as a conjugate fault of the Yamada fault, has high micro-seismicity which extends to the Japan Sea off Tango Peninsula (OIKE, 1976; WATANABE *et al.*, 1984). The micro-seismicity, in the northern part of Kinki district, seems to be less in the granitic region than in the Mesozoic to Paleozoic sedimentary rocks.

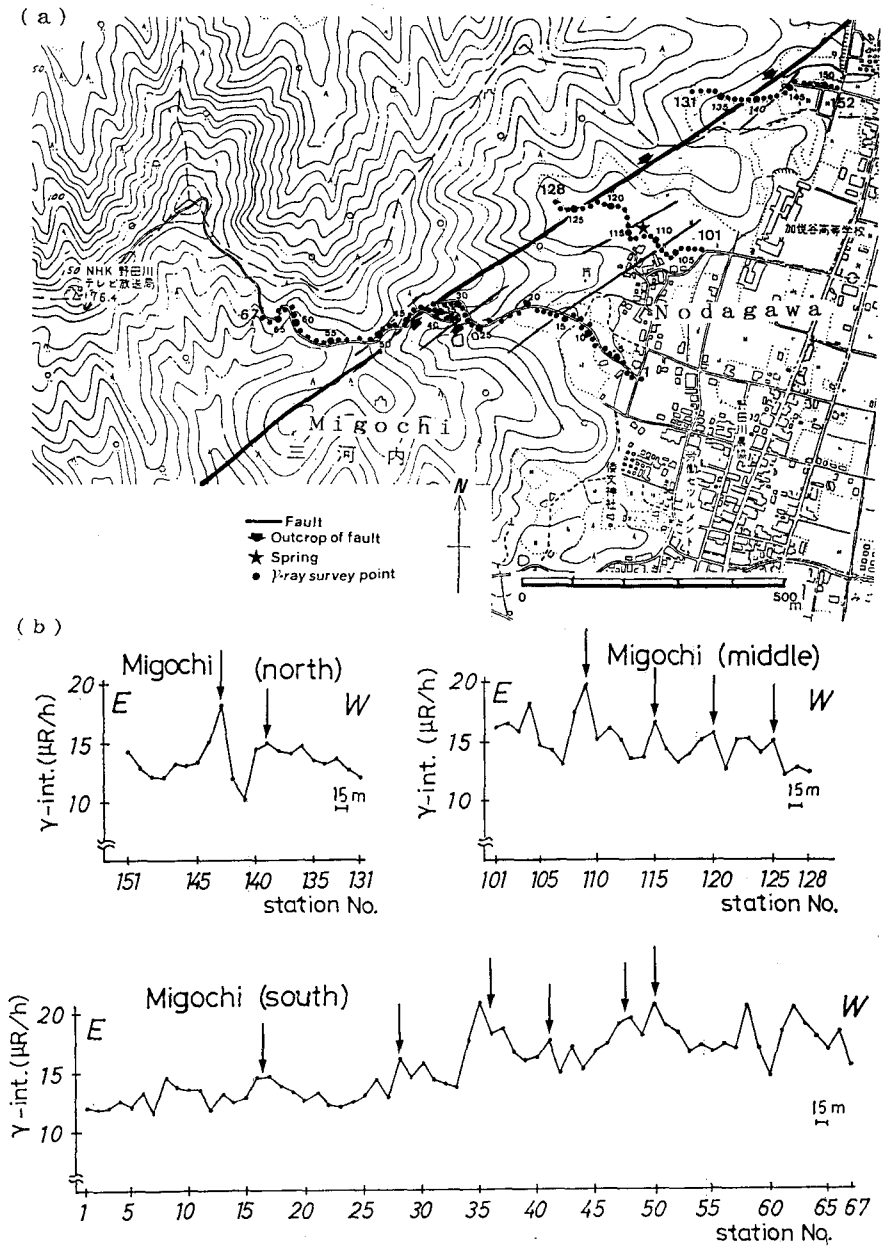

Fig. 25. Examples of γ-ray profiles at the surveyed lines across the southwest extension of Yamada fault in Nodagawa area (after KATSURA *et al.*, 1987a). Arrows show the possible positions of fault plane at surface. (a) map and (b) profiles.

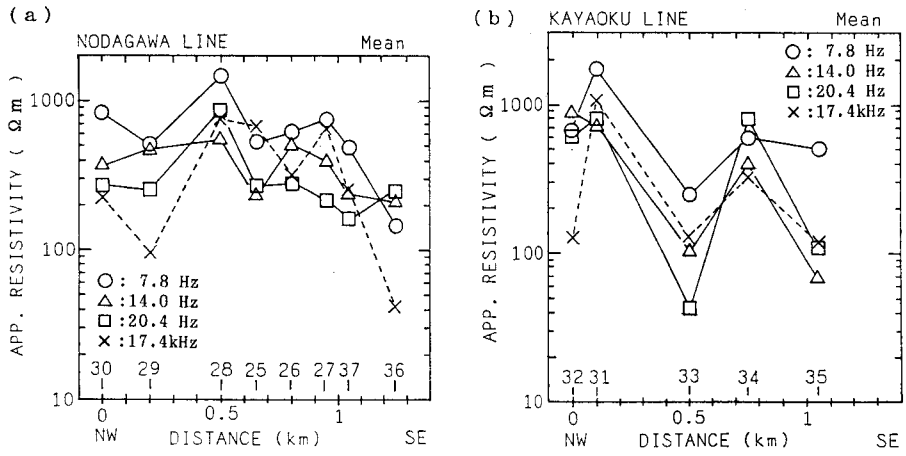

Fig. 26. NW-SE mean apparent resistivity profiles of ELF-MT soundings across the southwest extension of Yamada fault at Nodagawa area (after KATSURA *et al.*, 1987a). (a) Nodagawa line and (b) Kayaoku line. ELF-MT sites are shown in Fig. 24(c).

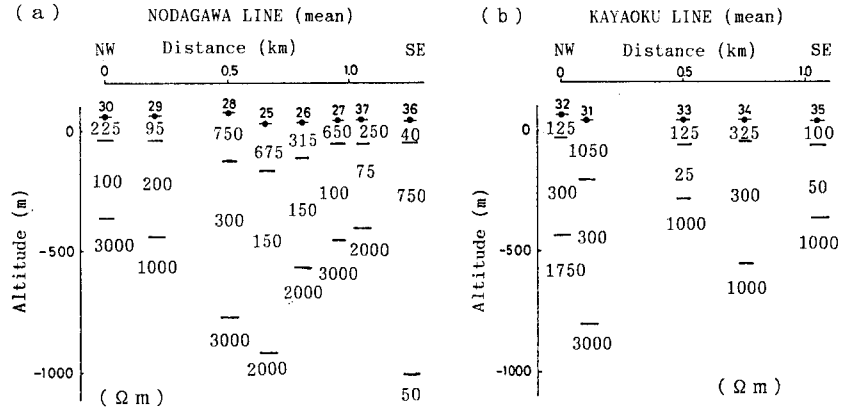

Fig. 27. NW-SE resistivity sections across the southwest extension of Yamada fault at Nodagawa area after one-dimensional analysis (after KATSURA *et al.*, 1987a). (a) Nodagawa line and (b) Kayaoku line. ELF-MT sites are shown in Fig. 24(c).

Both the Yamada and Gomura faults run mainly in the granitic rock massif. The difference of seismicity between these two faults suggests the difference of stress field acting to the fault zones. In other words, the angle between the strike of fault and the maximum axis of regional stress field should be involved. Assuming to an E-W maximum of stress, the zone of Gomura fault faces to a force with high angle.

3.6. The Hanaori Fault

The ELF-MT survey across the Hanaori fault had been performed in the coarse

site array by HANDA and SUMITOMO (1985). The ELF-MT survey in the series of this study was carried out to precisely discover the extent of fracture zone (YAMADA *et al.*, 1989). Typical two-dimensional structure of this fault is proper to test the validity of ELF-MT method for the survey of active fault. Then the two-dimensional analysis using the FEM was applied to this fault.

The Hanaori fault is a major fault with about 60 km of extension in the northern Kinki district (Fig. 1). The strike is about N20°E and the displacement is mainly right-lateral strike-slip. In some parts, the west side is depressed. This fault runs through old sedimentary rocks mainly composed of chert and shale and makes a boundary of geologic units. The west side is exposed by Mesozoic to Paleozoic sedimentary rocks called the Tamba belt. The east side is exposed by Cretaceous granitic rocks at Hira and Hiei mountains behind narrow exposure of the Tamba belt. The micro-seismicity is high active along this fault.

The survey sites were arranged along two lines perpendicular to the strike of fault (Fig. 28). The apparent resistivity profile is made by the join of two profiles taken from Boumura and Nakamura lines because the sites of two lines at the Ado River showed similar apparent resistivities (Fig. 29). The two-dimensional analysis was applied to the results after the one-dimensional analysis. The model section after the two-dimensional analysis is presented in Fig. 30. The fracture zone along the Hanaori fault is estimated to about 1.4 km of width. The depth of fracture zone

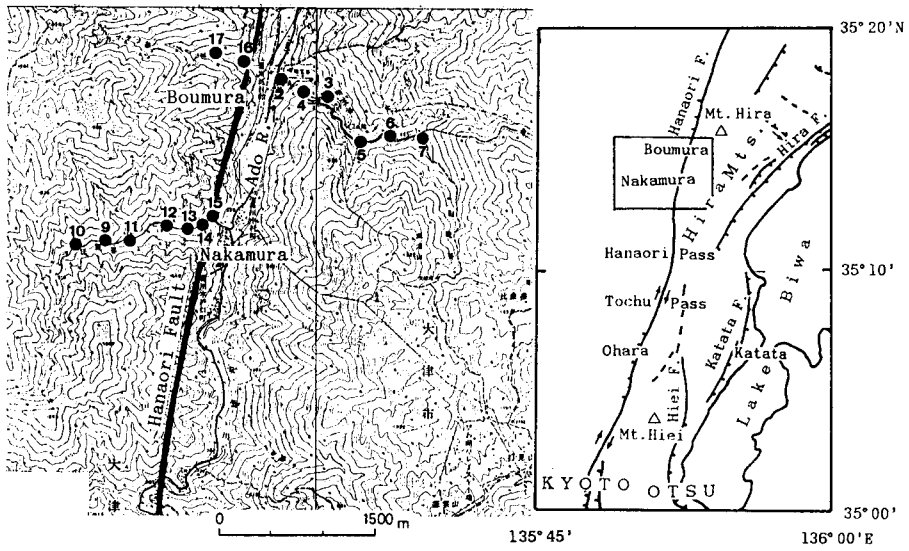

Fig. 28. Location of survey sites of ELF-MT soundings at the Hanaori fault (after YAMADA *et al.*, 1989).

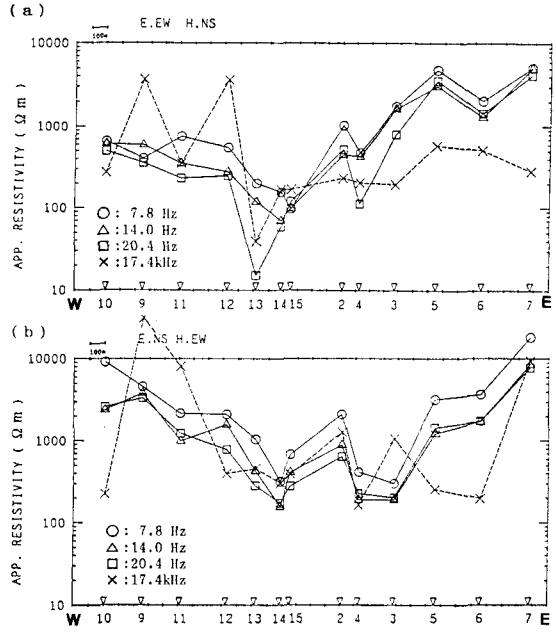

Fig. 29. E-W apparent resistivity profiles of ELF-MT soundings across the Hanaori fault (after YAMADA *et al.*, 1989). Surveyed sites are shown in Fig. 28. The profile is joined to Boumura and Nakamura lines at Ado River. (a) TM-mode. (b) TE-mode.

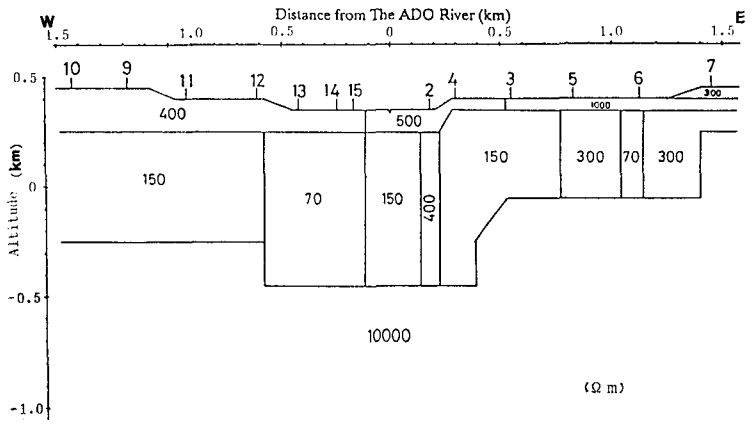

Fig. 30. E-W resistivity section across the Hanaori fault after the two-dimensional analysis (after YAMADA *et al.*, 1989). Surveyed sites are shown in Fig. 28.

is more than 800 m. The shape of section of fracture zone is approximately rectangular and centered on the Ado River. The densely fractured zone exists along the west side of the Ado River as shown by 70 Ωm zone of resistivity. The detail interpretations on the resistivity structure are given in YAMADA *et al.* (1989).

3.7. Northwestern Coast of Lake Biwa

The Bouguer anomaly map around Lake Biwa (Fig. 11) reveals three regions of remarkably low anomaly off Takashima, off Imazu and at Nishi-Azai. The chain of low anomaly along the west coast of Lake Biwa seems to be parallel to the chain of faults from the Katata and the Hiei-Hira faults to the Aibano fault. And the trend of low anomaly seems to be traced to Tsuruga.

The northern coast of Lake Biwa is known to have a complicated fault structure (TOGO, 1974; MURAI and KANEKO, 1975). The area is probably bounded by the

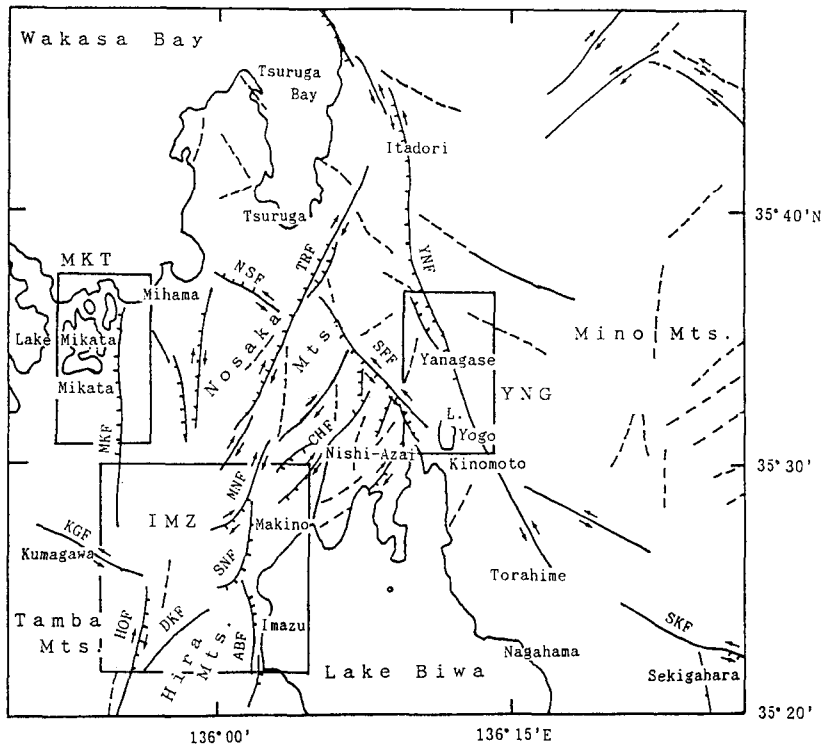

Fig. 31. Distribution of active faults in the northern area of Lake Biwa (modified from MURAI and KANEKO, 1975 and R.G.A.F., 1980). YNF: Yanagase fault, SKF: Sekigahara fault, TRF: Tsuruga fault, SFF: Shufukuji fault, NSF: Nosaka fault, CHF: Chihara fault, MNF: Makino fault, SNF: Sanami fault, ABF: Aibano fault, DKF: Dokenyama fault, HOF: Hanaori fault, KGF: Kumagawa fault, MKF: Mikata fault. IMZ: Imazu, YNG: Yanagase, MKT: Mikata areas.

Kumagawa fault-Imazu line, the Yanagase fault and the Mikata fault (Fig. 31). The faults make a conjugate system in which the NE-SW striking fault is right-lateral strike-slip and the NW-SE striking fault is left-lateral. The low Bouguer anomaly around Nishi-Azai is situated in this area.

The cause of low gravity anomaly and dense distribution of fault system is partly considered to be the depression of Mohorovičić and Conrad discontinuities (HURUKAWA, 1983) at the west of Lake Biwa relative to the mountainous regions. The severely crushed rocks at this region could also contribute to the low anomaly (NISHIDA *et al.*, 1990).

The geophysical exploration around this area was planned to search location of

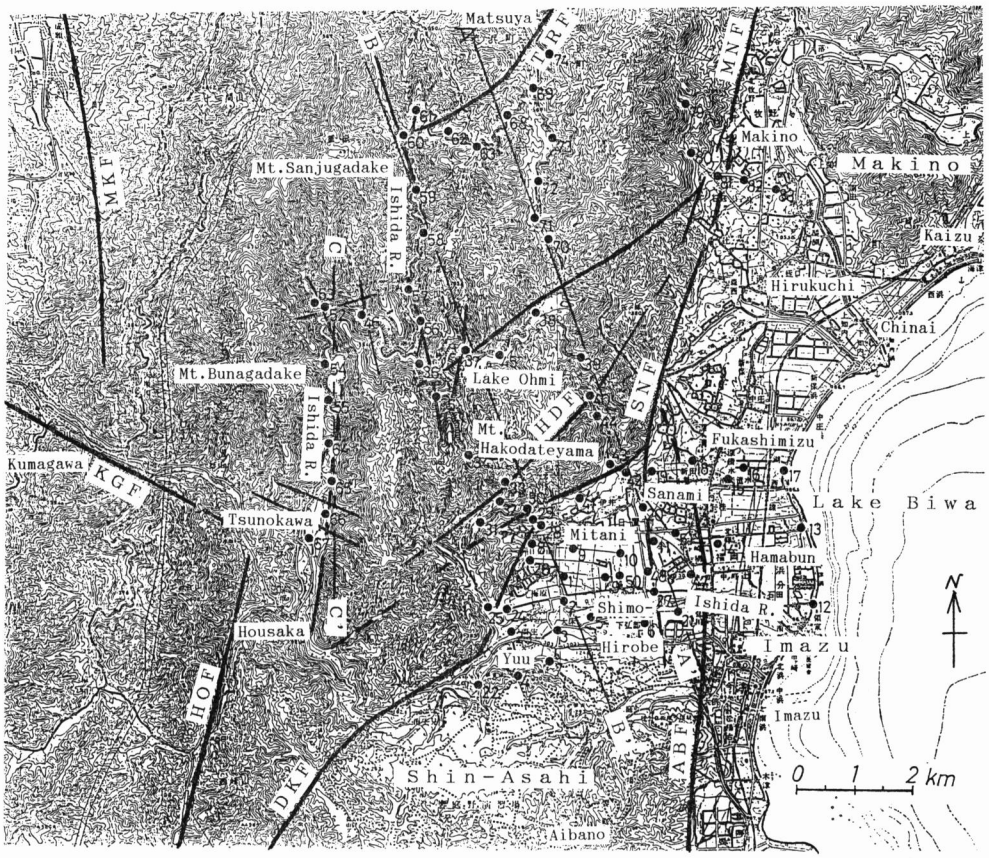

Fig. 32. Location of ELF-MT sites (solid cricle) and estimated faults (bold line) around Imazu and its vicinity, northwestern coastal area of Lake Biwa. TRF: Tsuruga fault, MNF: Makino fault, SNF: Sanami fault, ABF: Aibano fault, DKF: Dokenyama fault, HDF: Hakodateyama fault, HOF: Hanaori fault, KGF: Kumagawa fault, MKF: Mikata fault.

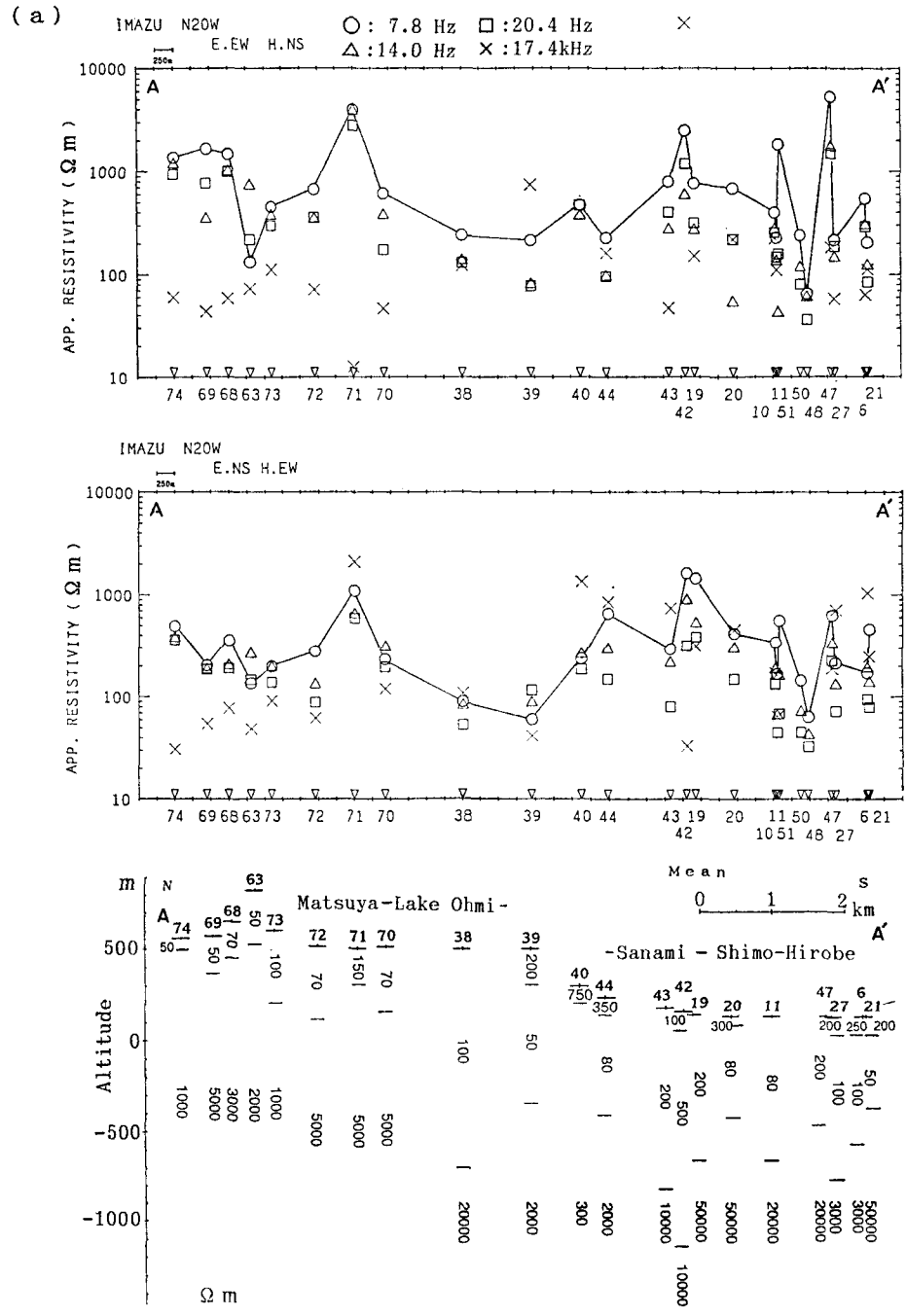
(a)
IMAZU N20W
E.EW H.NS
○ : 7.8 Hz □ :20.4 Hz
△ :14.0 Hz × :17.4kHz
APP. RESISTIVITY (Ω m)
A
A'
74 69 68 63 73 72 71 70 38 39 40 44 43 19 20 11 50 47 21
42 10 51 48 27 6
IMAZU N20W
E.NS H.EW
m
N
Matsuya-Lake Ohmi-
-Sanami - Shimo-Hirobe
Mean
0 1 2 km
Altitude
500
0
-500
-1000
Ω m

Fig. 33 (a)

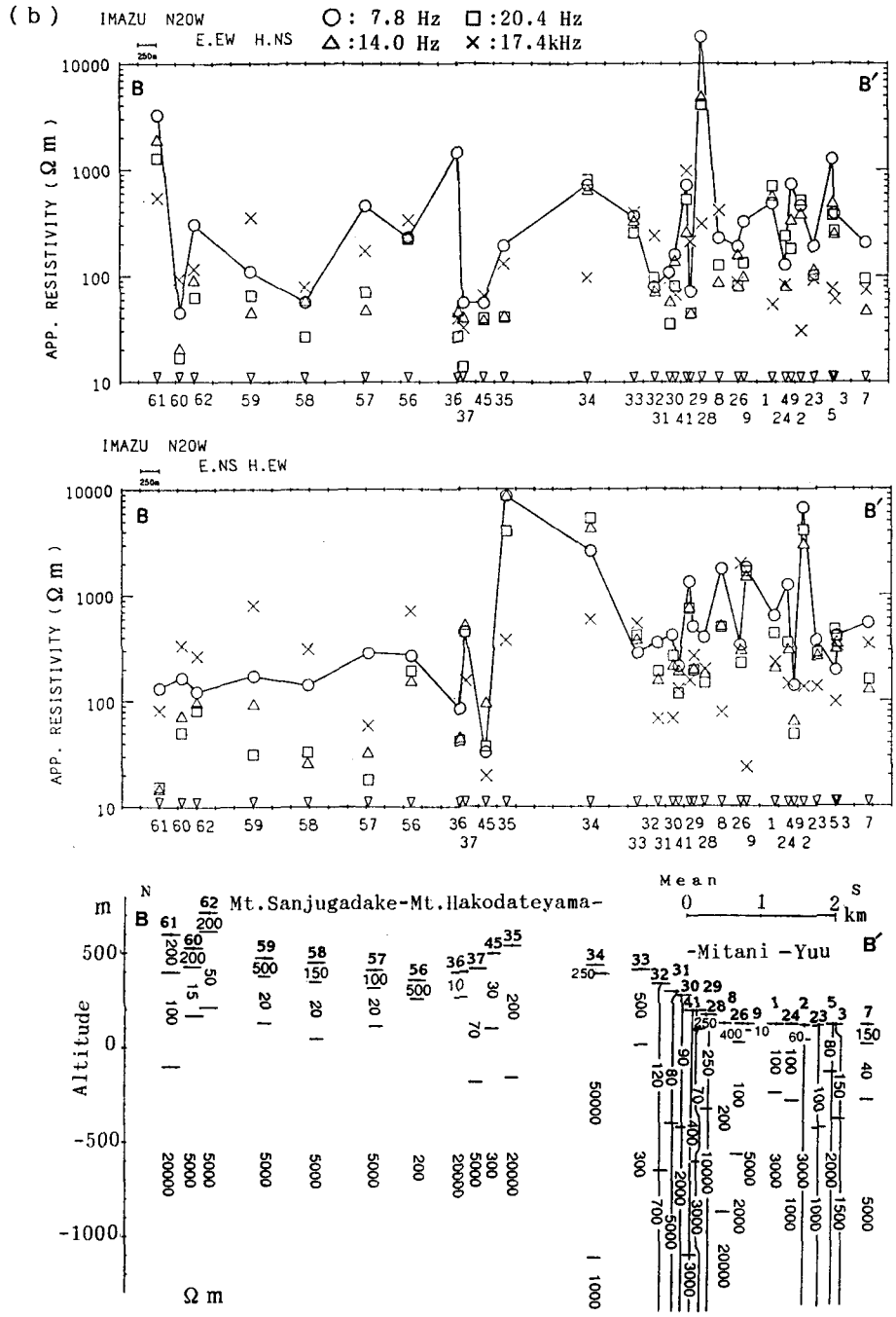
(b)
IMAZU N20W
E.EW H.NS
○ : 7.8 Hz □ :20.4 Hz
△ :14.0 Hz × :17.4kHz
APP. RESISTIVITY (Ω m)
B
B'
IMAZU N20W
E.NS H.EW
Mean
Mt.Sanjugadake-Mt.Hakodateyama-
-Mitani -Yuu
Altitude
m
Ω m

Fig. 33 (b)

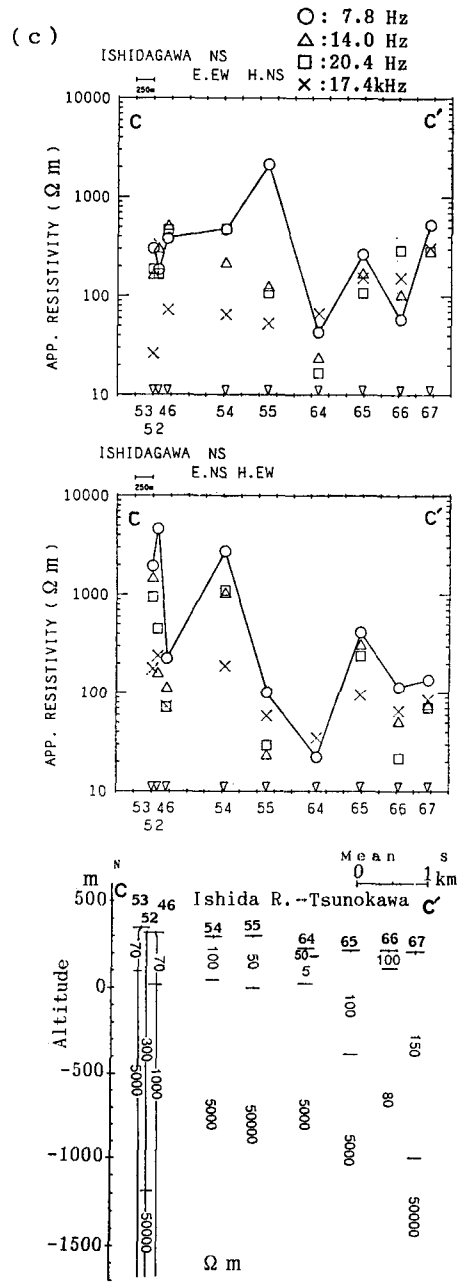

Fig. 33 (c)

Fig. 33. Apparent resistivity profiles of ELF-MT soundings and resistivity sections (mean) after one-dimensional analysis around Imazu and its vicinity. Site positions and projected lines are shown in Fig. 32. (a) Line A-A' from Matsuya to Shimo-Hirobe through Sanami. (b) Line B-B' from Mt. Sanjugadake to Yuu through Mt. Hakodateyama and Mitani. (c) Line C-C' along Ishida River.

major fractures. The methods employed are ELF-MT and γ-ray. Here, the results at Imazu and its vicinity (Fig. 31) are presented.

In this area, there are many power lines of high voltage. Therefore, the receiver site of ELF-MT sounding using natural electromagnetic waves was strongly restricted. Fig. 32 shows distribution of ELF-MT sites and the estimated faults. The results of ELF-MT survey is presented in Fig. 33. As the mode separation between TM and TE was hardly successful, the one-dimensional analysis was applied to the mean apparent resistivities. The profiles and one-dimensional solutions suggest the

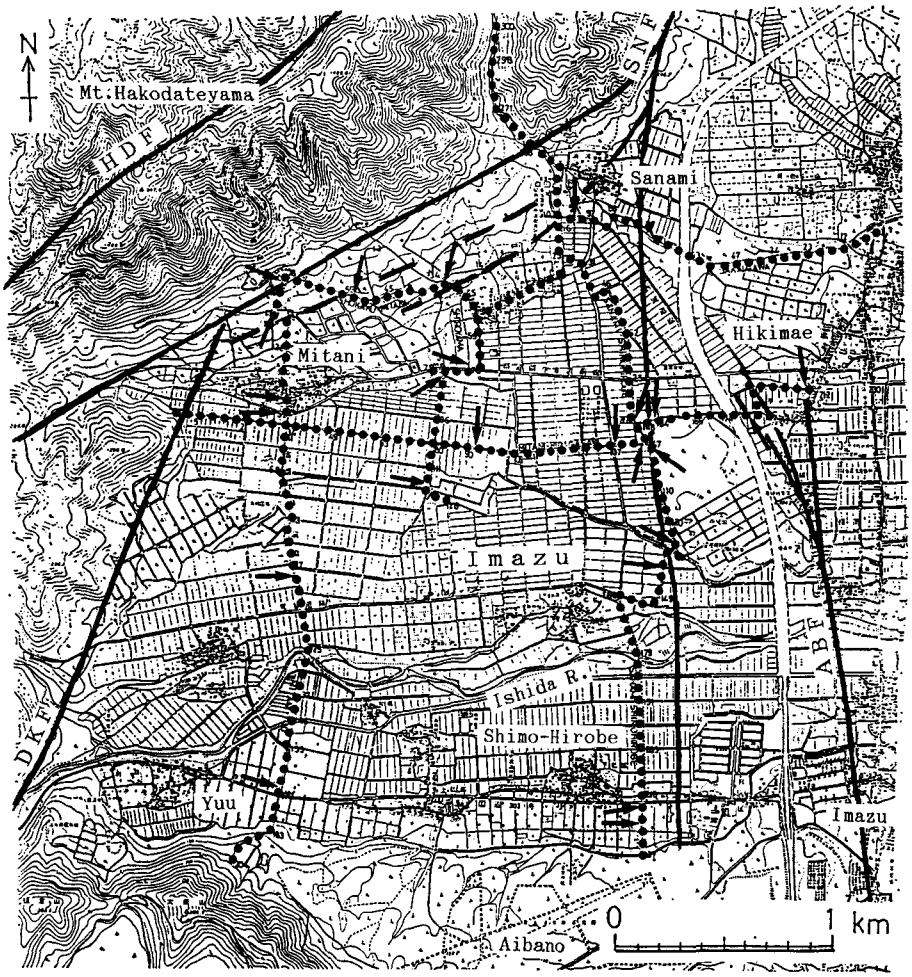

Fig. 34. γ-ray survey lines (dotted line) at Imazu. Arrows indicate the points showing high level intensity of γ-ray. Solid lines show estimated fault lines. ABF: Aibano fault, SNF: Sanami fault, HDF: Hakodateyama fault, DKF: Dokenyama fault.

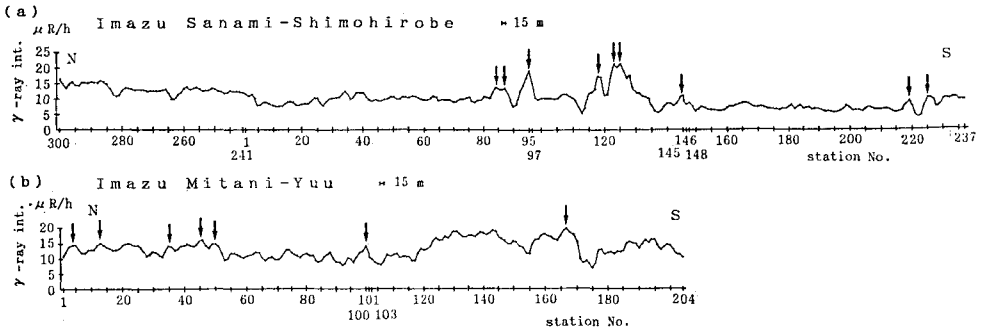

Fig. 35. Examples of γ-ray profiles at Imazu. Survey lines are shown in Fig. 34. The data are after smoothing for five points. (a) N-S line from Sanami to Shimo-Hirobe. (b) N-S line from Mitani to Yuu.

existence of several fracture zones with about NE-SW and N-S strikes. The trend of faulting seems to be along the valleys in the mountainous region.

The γ-ray survey was carried out in the Imazu plain. The survey points are shown in Fig. 34 and the results of typical lines are shown in Fig. 35. The points where the γ-ray intensity is relatively high make linear arrays. One is an N-S striking array parallel to the Aibano fault and another is along the foot of Mt. Hakodateyama with ENE-WSW strike.

The fault distribution is estimated from the results of ELF-MT and γ-ray surveys with reference to the geological and the topographical evidences. The estimated faults are shown in Fig. 32. The fractured zones spread widely and extend for NE-SW and N-S directions. There is a possibility of existence of densely crushed basements. The rock types exposed in this region is mainly hard sedimentary rocks as the Tamba belt. These structures are reflected from the lithological factor and the stress convergence at this region.

The newly estimated portions are as follows; (1) south extension of the Sanami fault parallel to the Aibano fault, (2) southwestern branch of the Sanami fault through the foot of Mt. Hakodateyama, (3) northeast extension of the Dokenyama fault to reach to the branch of Sanami fault, (4) southwest extension of the Makino fault to the Lake Ohmi, (5) trace of the Hakodateyama fault, (6) southwest extension of the Tsuruga fault from Matsuya to Mt. Sanjugadake, (7) some signs of faulting along the Ishida River.

3.8. The Mikata Fault

The Mikata fault is an N-S striking active fault (Fig. 31) with a vertical displacement of the eastern side uplift (MIURA *et al.*, 1969 referred in MURAI and KANEKO, 1975). The amount of displacement is unknown. Geophysical exploration on this fault has been carried out with the γ-ray, gravity and resistivity (Wenner array)

Fig. 36. Location of ELF-MT survey sites across the Mikata fault. Solid lines show the fault lines. MKF: Mikata fault.

methods by HATUDA *et al.* (1961, 1965 unpublished). An ELF-MT survey was carried out in the present study across the fault (Fig. 36).

Apparent resistivity profile and resistivity section are presented in Fig. 37. The estimated position of main fracture zone (around the site 6) inferred from the ELF-MT method is slightly west (about 200 m) from the former result of fault line estimated by HATUDA *et al.* and from the geological and topographic features. Furthermore, it is considered that there is a wide fracture zone below the region west of the site 3. Although the western boundary of the fracture is obscure, it may be at the site 11.

3.9. The Yanagase Fault

The Yanagase fault is a major active fault with a strike of NNW-SSE (Fig. 31) (SUGIMURA, 1963; MURAI and KANEKO, 1975; R.G.A.F., 1980). The elongation is recognized as about 25 km from Kinomoto to Itadori. The fault displacement is principally vertical and the east side is relatively uplifted. Left-lateral strike-slip is also recognized. The fracture zone is about 150 m to 300 m of width at the north end near Itadori and the width of 30 m to 50 m is strongly fractured (IKEDA, 1958;

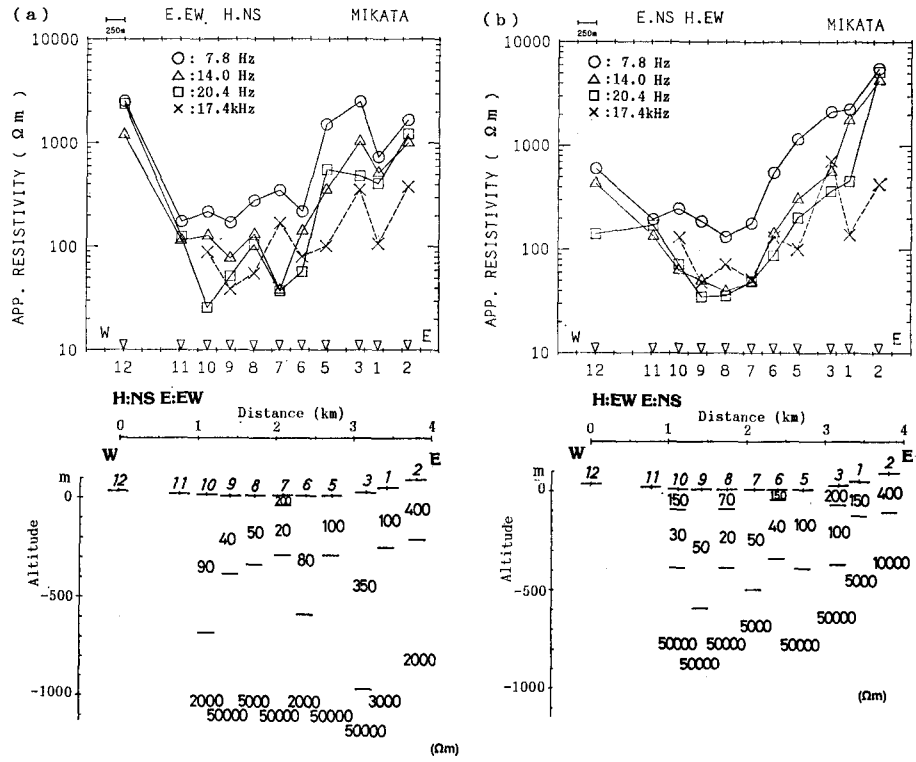

Fig. 37. E-W apparent resistivity profiles and resistivity sections across the Mikata fault. Surveyed sites are shown in Fig. 36. (a) TM-mode, (b) TE-mode.

TAKAHASHI and SHIRAI, 1959 referred in SUGIMURA, 1963 and MURAI and KANEKO, 1975). The Anegawa earthquake (August 14, 1909; *M*6.8; epicenter 136.3°E, 35.4°N [UTSU, 1982]) is considered to be caused by the displacement, principally east side uplift, of the hidden fault as the auxiliary parallel fault of the Yanagase fault (SUGIMURA, 1963). The Yanagase fault, furthermore, is considered to be a major tectonic boundary as the eastern border of the Kinki triangle region (HUZITA *et al.*, 1973). An additional geophysical exploration on this fault is meaningful to test the sensitivity of the survey method.

An ELF-MT survey was carried out along a survey line across the Yanagase fault at the central part near Yanagase (Fig. 38). The apparent resistivity profile and resistivity section are shown in Fig. 39. Although the receiving of ELF noise at the valley of fracture zone was unsuccessful for the disturbing by power line, the low resistivity zone was found at the point 1 km east of the fault valley. This point (at the site 7) is located at a pass of the mountain chain parallel to the fault valley. And an outcrop of the fracture is recognized. It is considered that the fracture

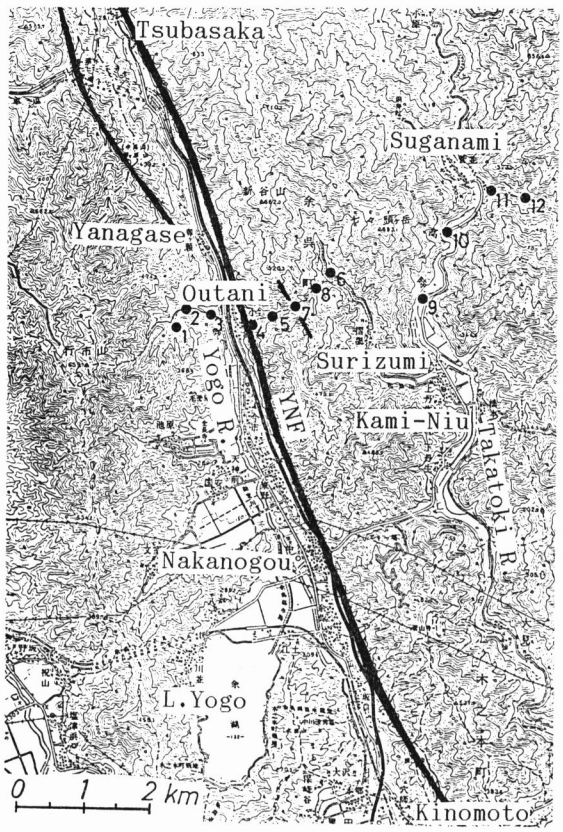

Fig. 38. Location of ELF-MT survey sites across the Yanagase fault. Solid lines show the fault lines. YNF: Yanagase fault.

occurs along several parallel faults such as this example.

4. Block Structure in the Northern Part of Kinki District

Major active faults should be chained up in the hidden areas according to the results of the surveys. Fig. 40 shows a joined fault system in the northern part of Kinki district. Typical chains of the faults can be recognized as follows: The first consists of the ATL, the Jumantsuji fault, the STL and the Yamasaki fault, and faces to the Ute fault. The second consists of the Yagi, the Yabu and the Mitoke faults, and perhaps approaches to the Nishiyama fault. The third consists of the Mikata and the Hanaori faults, and reaches to the MTL through the Ikoma or the Miyakata fault. The fourth consists of the Yanagase, the Yoro and the Ise-Bay faults. The fifth consists of the Kizugawa fault, and is perhaps linked with

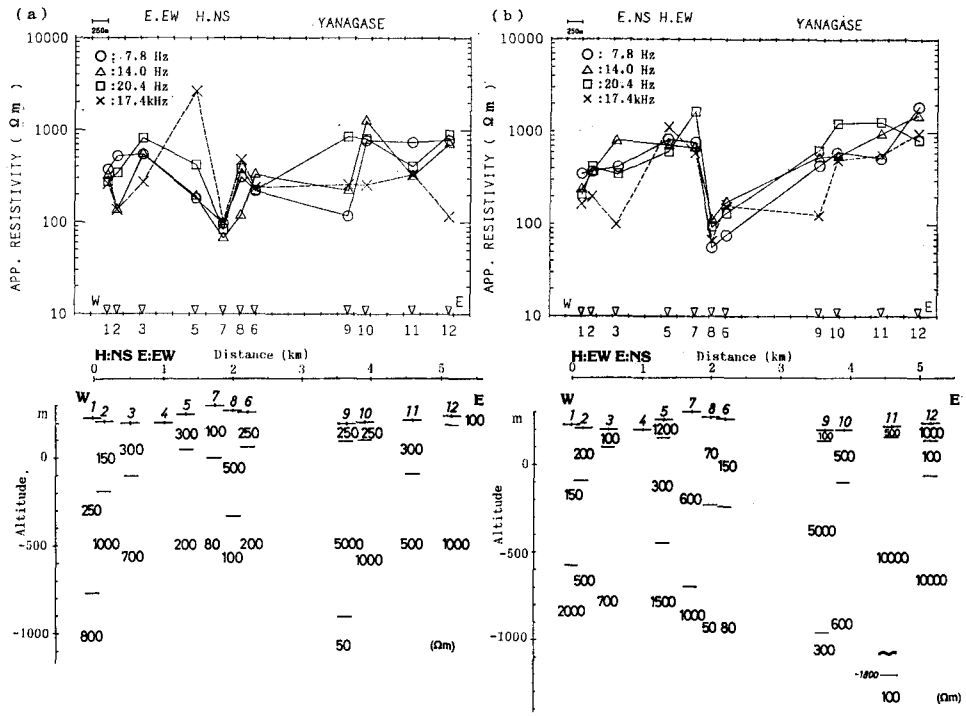

Fig. 39. E-W apparent resistivity profiles and resistivity sections across the Yanagase fault. Surveyed sites are shown in Fig. 38. (a) TM-mode, (b) TE-mode.

the Fujiwaradake fault or the Suzuka fault.

The enclosed area bounded by these chains of active faults is considered to be a tectonic unit tentatively named the tectonic block. In the northern part of Kinki district where is north of the MTL, we can tentatively assume seven tectonic blocks which are named the Tamba, the Harima, the Hokutan, the Maizuru, the Biwa-ko, the Nara and the Osaka blocks (Fig. 40). For the definition of block boundaries, we should refer to the micro-seismicity (Fig. 41), because the seismic activity is closely related to the activity of active fault. If a new discovery of large fracture zone of a hidden active fault was added, the location of block boundary and the number of blocks would be modified in the future. The sea-side boundaries, which are undefinable at the present time, are the future problems to be examined.

Boundaries of tectonic blocks are not necessarily corresponding to the geological boundaries. Fig. 42 shows a geological map of the northern part of Kinki district. Major active faults sometimes run through a geologic unit. Examples of this case are seen in the Mitoke and the Yamada faults. However, the boundaries often correspond to the transition zones of geologic and topographic features. The geo-

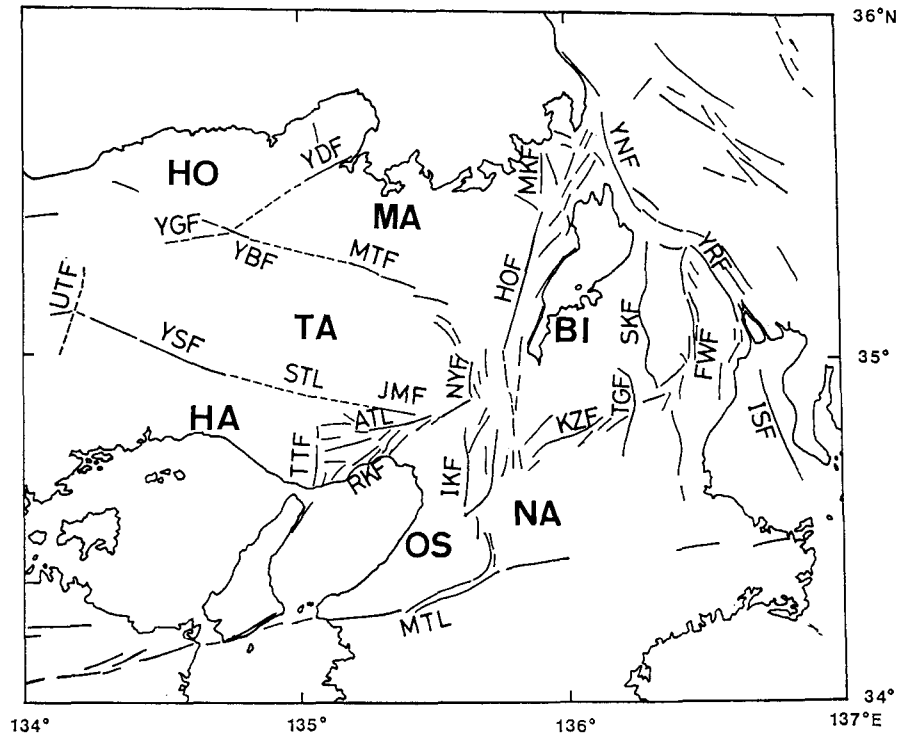

Fig. 40. Distribution of tectonic blocks in the northern part of Kinki district. Major active faults are shown by bold line for the known part before this study and by broken line for the discovered part in this study. HO: Hokutan block, MA: Maizuru block, TA: Tamba block, BI: Biwa-ko block, NA: Nara block, OS: Osaka block, HA: Harima block. STL: Sanda-Yamasaki Tectonic Line, UTF: Ute fault. Other faults are represented by the same codes as those of Fig. 1.

logic character, especially rock type of basement, is conspicuous in the tectonic response of each block. The response is seen in the seismicity of intra-block (see Fig. 41). The transition zone of topography on the manner of mean altitude is considered to relate the occurrence of earthquakes (MINO, 1984). The Yamasaki fault system is its example. The northern side of this fault is higher than the southern side. Since the topography is the result of the tectonic activity and is dependent on the lithologic character, the consistency between the block boundary and the topographical transition zone suggests the validity of block boundary in the tectonics.

Each block can, therefore, be characterized from the viewpoints of geology and seismology. The description of each block is presented below:

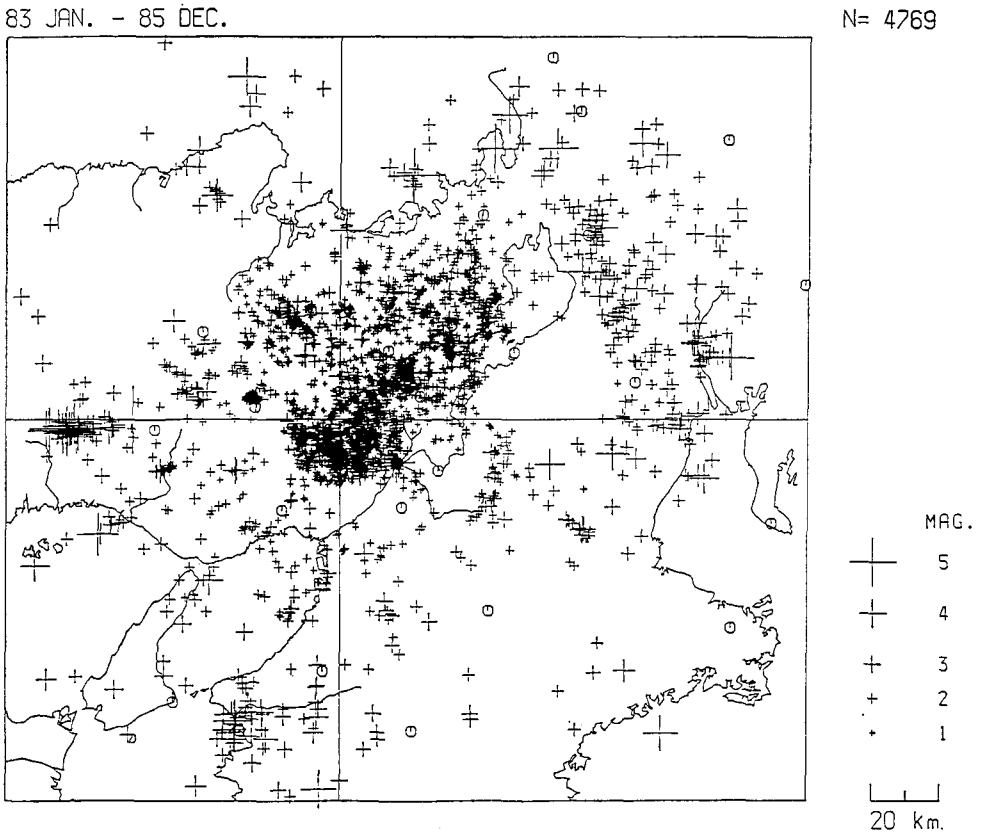

Fig. 41. Seismicity map of the northern part of Kinki district during the dates from January, 1983 to December, 1985 (after ABUYAMA SEISMOLOGICAL OBSERVATORY). Cross is position of epicenter and its size is proportional to magnitude. Focal depth is shallower than 30 km.

4.1. The Tamba Block

This is the most definable tectonic block of its boundary. Our clear results of hidden active faults mainly gather around this block (MOGI *et al.*, 1985a, b; KATSURA *et al.*, 1987a, 1989). The southern and the northern boundaries are the first and the second above-mentioned chains, respectively. The western boundary is considered to be the Ute fault. However, the eastern boundary at the Kyoto basin is not definitely known yet. One possibility is the Nishiyama fault and another is the chain of the Hanaori and the Obaku faults.

The basement of this block is Permian to middle Mesozoic Tamba belt mainly composed of hard compressed sedimentary rocks, such as chert and shale. In the southwestern part, rhyolitic rocks are widely exposed at the surface. Eastern part

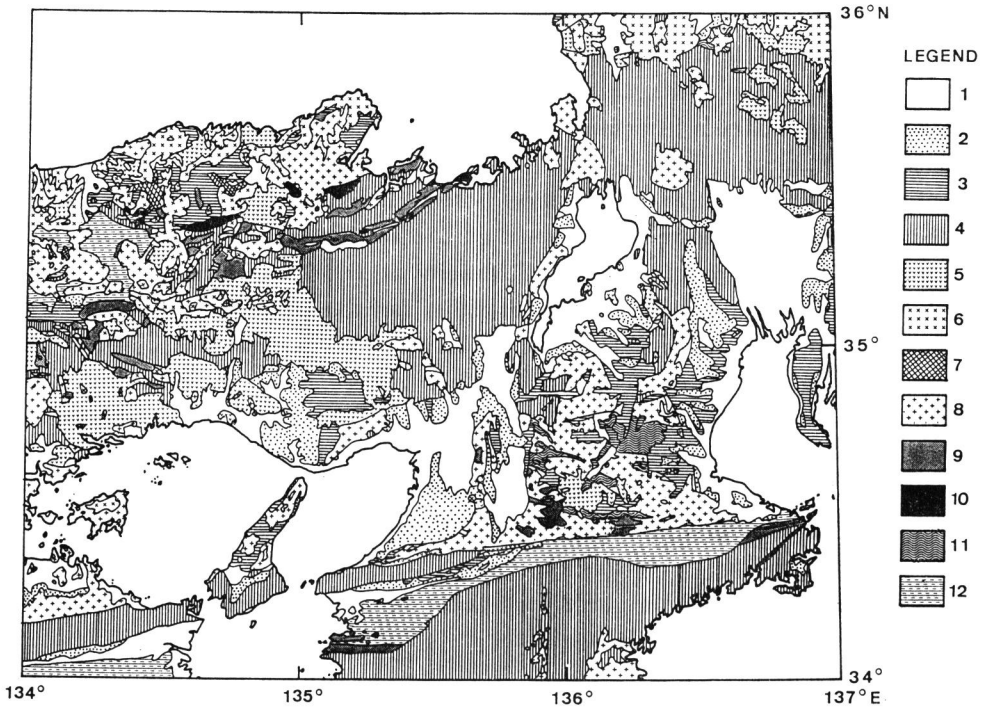

Fig. 42. Geological map of the northern part of Kinki district (modified from YAMADA *et al.*, 1982). 1: Holocene sediments, 2: Pleistocene sedimentary rocks, 3: Neogene sedimentary rocks, 4: Pre-Neogene sedimentary rocks partly includes basalt, 5: rhyolite and dacite, 6: andesite and basalt, 7: alkali basalt, 8: granitic rocks, 9: gabbro and diorite, 10: ultramafic rocks, 11: low-pressure type metamorphic rocks, 12: high-pressure type metamorphic rocks.

is the region where the micro-seismicity is the most active (Fig. 41). The Tamba belt near Kyoto is considered to be densely fractured or to be fast deformed (OIKE, 1976). On the contrary, the northwestern border along the Yagi fault is a quiet boundary in the view of seismicity. This fact may be partly attributed to the serpentinite body situated along the south side of the fault, because we assume the release of stress in the hydrated layer of serpentine.

4.2. The Harima Block

This block lies to the south of the Tamba block. The western border is not defined. The eastern border is the Takatsukayama fault or an assemblage of the faults at the southeast foot of the Rokko mountains such as the Rokko fault system.

The basement is probably of the Tamba belt. The surface is mainly exposed by rhyolitic to granitic rocks and Neogene to Quaternary sediments.

4.3. The Hokutan Block

This block lies to the north of the Tamba block bounded by the Yagi fault. The boundary between this and the Maizuru block is the Yamada fault system. The western boundary is tentatively assumed to be the line from Tottori to the Ute fault through Chizu.

In this block, Neogene sedimentary rocks including volcaniclastics are exposed widely. Granitic rocks are also exposed in the eastern part. The Yamada fault system runs in the granitic region. Seismicity at the intra-block and the block border concentrates along the Gomura and the Yamada faults. And the seismicity along the Gomura fault extends to the Japan Sea (WATANABE *et al.*, 1984). The seismicity along the northwestern coast of the Tango Peninsula is seen on the linear distribution of epicenters from the Shikano and the Yoshioka faults, at the west of Tottori, to here through a seismicity gap at the northern part of Hyogo Prefecture (OIKE, 1976; WATANABE *et al.*, 1984). Furthermore, a peculiar point of this block is that there are several occurrences of intra-block large earthquakes ($M \geqq 6.0$ class), such as the Kita-Tajima earthquake (May 23, 1925; $M6.8$; epicenter 134.8°E, 35.6°N [UTSU, 1982]) and the $M6.3$ earthquake occurred on January 20, 1949 (epicenter 134°32′E, 35°37′N) (J.M.A., 1982).

4.4. The Maizuru Block

This block is adjacent to the Tamba, the Hokutan and the Biwa-ko blocks. The boundary between this and the Tamba block is the chain of the Yabu-Yagi and the Mitoke faults. The boundary between this and the Biwa-ko block is the Hanaori fault, but the northern part of this boundary is not clear. The Mikata fault is its strong candidate.

Main rock types of the basement of this block are hardly compressed sedimentary rocks as in the Tamba belt. In the northern part, there are the sedimentary Maizuru group and the Yakuno complex including ultramafics, and partially granitic rocks. The intra-block seismicity is active in the Tamba belt region and more active in the southernmost region.

4.5. The Biwa-ko Block

This block lies to the east of the Tamba and the Maizuru blocks and to the north of the Nara block. The western boundary is the Hanaori fault and its extension to the Wakasa Bay probably through the Mikata fault. The eastern boundary is the Yanagase fault. The boundary between this and the Nara block is probably the Kizugawa fault which induced a displacement at the $M 7\frac{1}{4}$ earthquake on July 9, 1854 (epicenter 136.0°E, 34.75°N [USAMI, 1987]). However, the boundary at the southeast side is not clear. The Yoro fault is the most probable boundary

because the seismicity concentrates on this fault. On the other hand, the Fujiwaradake and the Suzuka faults are alternative candidates of the boundary, but the Fujiwaradake fault is more probable.

The most remarkable feature of this block is that there is a deep sedimentary basin of the Lake Biwa. Surrounded areas are exposed by granitic to rhyolitic rocks where the intra-block micro-seismicity is quiet, especially in the southern half as the plain east to the Lake Biwa. The basement, however at least in the northern half, is hard compressed sedimentary rocks as the Tamba and the Mino belts. In other words, this block is composed of soft thick covers and hard basement on the viewpoint of mechanical property. Furthermore, the area enclosed by the Wakasa Bay, the Yanagase fault, the Mikata fault, and the north of Lake Biwa basin is a densely fractured zone.

4.6. The Nara Block

This block is situated to the south of the Tamba and the Biwa-ko blocks and to the east of the Osaka block. The northern boundary between this and the Tamba block is complicated. There is no significant lineament with E-W sense between the Kizugawa fault and the Ikoma fault. However, the geological character is different from that of the Tamba block. There are mainly granitic rocks as the Ryoke complex and the Neogene strata and volcanics.

The western boundary is probably the chain of the Ikoma fault and the faults at the east foot of the Kongo-Katsuragi mountains through the Yamatogawa fault. Lastly, it faces to the MTL. A bend in the western boundary seems to be reasonable on the seismic activity, especially on the historical earthquakes. However, we must remember the Miyakata fault (see Fig. 13 and Fig. 14). For the present, we could not decide which faults, the Ikoma, the Miyakata or the other fault, was a major one. Furthermore, the eastern boundary is probably the chain of the Yoro and the Ise-Bay faults. There is a little possibility of the Tongu fault as the boundary, because the epicentral distribution is recognizable as linear.

4.7. The Osaka Block

The Osaka block includes the Osaka plain and the Osaka Bay. The surface of this block is characterized as thick loose sediments of the Quaternary. The basement is probably the granitic Ryoke complex. The western boundary and the relation to the Awaji Island are obscure.

5. Tectonic Activity of Block Boundary

Mechanical state of the block structure model agrees qualitatively with the regional tectonic conditions. As mentioned above, the regional tectonic field in

the northern part of Kinki district is governed by the horizontally E-W to ESE-WNW compression caused by the subducting slab of the Pacific plate (*e.g.* HUZITA *et al.*, 1973). The pattern of the strikes of block boundaries makes principally a conjugate fault system. Displacements of the strike-slip faults participating in the block boundaries agree with the regional stress field. In the southern parts of the Tamba and the Biwa-ko blocks, the block boundaries are dominant in N-S strikes. The faults of these boundaries involve the displacement of reverse type and also concordant with the E-W compression.

In the first approximation, we could assume the tectonic block as a rigid body. In this sense, the regional tectonic stress must be consumed in the fracture zones at the block boundaries. On the higher approximation as a realistic case, the stress could not be consumed only at the block boundaries. Some parts of the stress are propagated into the block. The response of block is dependent on the mechanical property of its typical rock types. The response is clearly seen in the micro-seismicity of intra-block (Fig. 41). The micro-earthquakes of intra-block are considered to occur along the intra-block minor faults. The most vigorous response is seen in the eastern part of the Tamba belt composed of hard and compressed sedimentary rocks. On the contrary, the region composed of granitic basements is quiet in the seismicity. The relation between rock type and micro-seismicity is concordant with the general knowledge of mechanical responses of rocks under the confining pressure (*e.g.* HANDIN, 1966).

The activity of block boundary is monitored by the rate of fault displacement and by the seismicity along the boundary. The continuation of block boundary is from several tens kilometers to more than one hundred kilometers. The faulting of this scale is considered to be corresponding to the earthquake of magnitude above 6.0 class (MATSUDA, 1975). The recurrence time of earthquake is various from hundreds years to thousands years with respect to the magnitude and the size of fault. Here, the size of active fault means the area of fault plane; in other words, true length and depth including the hidden traces.

Now, let us compare the activity of block boundaries by using the record of large earthquakes. The reason for this procedure is that we consider the boundary of tectonic blocks to be a convergence front of the stress field. Thus, the release of stress could mainly occur at the block boundary. The compiled earthquake records show larger than $M5.5$ with some exceptions. When there is data on the depth of the focus, the earthquakes are confined to the shallow ones (depth less than around 30 to 40 km). The data of historical earthquakes before 1884 are from USAMI (1987). The data of recent earthquakes are from UTSU (1982, 1985) for 1885～1925, from J.M.A. (1982) for 1926～1960, and from Seismological Bulletins of J.M.A. (1962～1988) for after 1961.

For the historical large earthquakes, Fig. 43 shows the relation between the epicenters and the fault distribution. The epicentral locations include some errors. For the recent earthquakes, the error is about one or several minutes of latitude and longitude. For the historical ones, the error generally becomes larger as the occurrence is older. The error is probably less than 50 km and for most cases less than 25 km (USAMI, 1987). Taking account of the epicentral errors, we can say that the occurrence of large earthquakes is concentrated along the block boundaries. In this hypothesis, the limitation of magnitude of earthquakes is not clear. The $M5.5$ is a working assumption. Conversely, when we could collect many historically reliable records of large earthquakes, we may suppose the trace of block boundary, though we must confirm by the surveys.

The activity of block boundary is not necessary to be uniform through the historical past. Fig. 44 shows the occurrence time of historical large earthquakes with respect to the block boundaries. Historical activity of the block boundaries is de-

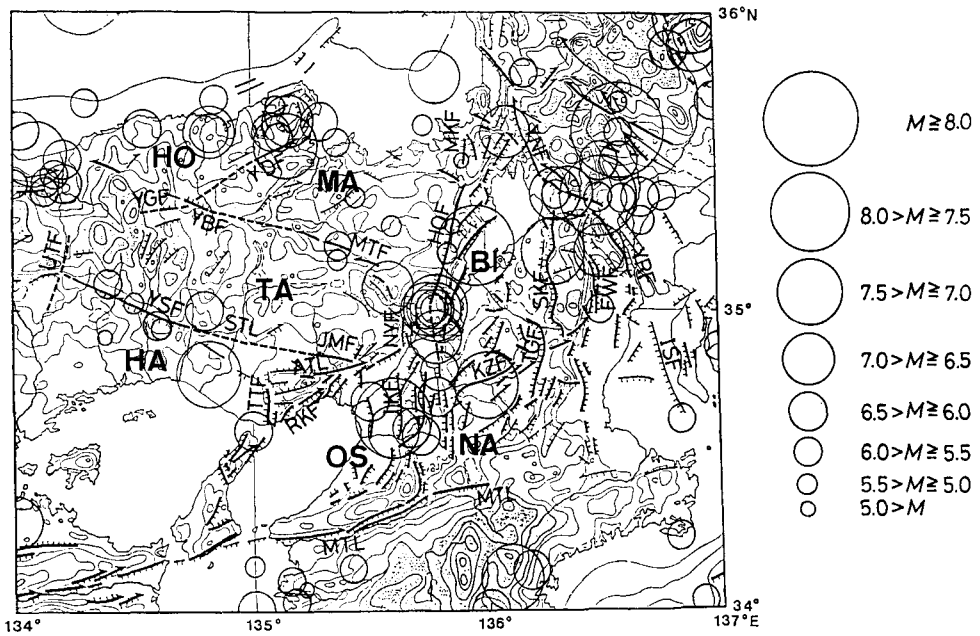

Fig. 43. Distribution of tectonic blocks, active faults and historical large and shallow earthquakes in the northern part of Kinki district. Active faults are shown by bold line with strike-slip or downthrown direction. Broken bold line is defined in this study. Open circle is historical large earthquake and diameter of circle is proportional to magnitude (J.M.A., 1982, 1962~1988; UTSU, 1982; USAMI, 1987). HO: Hokutan block, MA: Maizuru block, TA: Tamba block, BI: Biwa-ko block, NA: Nara block, OS: Osaka block, HA: Harima block. STL: Sanda-Yamasaki Tectonic Line, UTF: Ute fault. Other faults are represented by the same codes as those of Fig. 1.

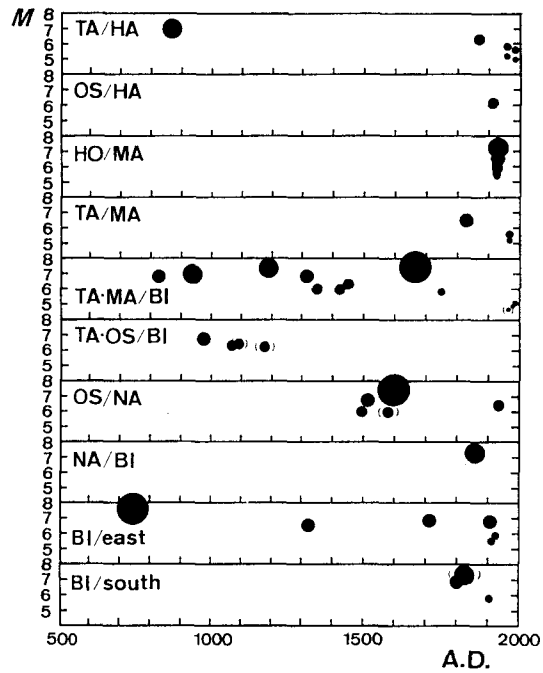

Fig. 44. Time-space plots of historical large earthquakes along block boundaries. Position and radius of solid circles are proportional to magnitude (J.M.A., 1982, 1962～1988; UTSU, 1982; USAMI, 1987). HO: Hokutan block, MA: Maizuru block, TA: Tamba block, BI: Biwa-ko block, NA: Nara block, OS: Osaka block, HA: Harima block. TA/HA: Yamasaki fault system including Sanda-Yamasaki Tectonic Line, OS/HA: Rokko and Takatsukayama faults, HO/MA: Yamada fault, TA/MA: chain of Mitoke, Kameoka and Nishiyama faults, TA·MA/BI: Hanaori and Mikata (in parentheses) faults, TA·OS/BI: Obaku and Ite (south extension of Obaku) faults and Sabota flexures (at north of Nara) (in parentheses), OS/NA: Ikoma, Yamatogawa (southeast extension of Ikoma) and Uemachi (at Osaka) (in parentheses) faults, NA/BI: Kizugawa fault, BI/east: Yanagase, Shufukuji and Sekigahara (between Yanagase and Yoro) faults, BI/south: Fujiwaradake and Suzuka (in parentheses) faults.

scribed for the five chains of active faults above-mentioned as follows:

Along the first chain, composed of the ATL, the Jumantsuji fault, the STL and the Yamasaki fault, large earthquakes often occurred. High activity of the micro-earthquakes is, of course, known. The most recent incident was the $M5.6$ earthquake on May 30, 1984, around the Goji fault (see Fig. 15), a southeast branch fault of the Yamasaki fault (J.M.A., 1985). The 868 Harima earthquake of $M \geqq 7.0$ seems to be distant from the block boundary (Fig. 43) (tentatively assumed by USAMI, 1987). However, the Harima earthquake is considered to be caused by the Yamasaki fault system. The ^{14}C dating for the bogwood recovered from fault region at Sanda, eastern part of the STL, shows $3{,}340 \pm 40$ years B.P. (NISHIMURA *et al.*, 1985). The

cultivated layer above the bogwood is not faulted. The last faulting is, therefore, estimated at the date between this ^{14}C date and the date of cultivated layer of about 400 years old. Furthermore, by trenching of the Yamasaki fault at Yasutomi (see Fig. 15), a vertical displacement has been disclosed which is supposedly caused by the Harima earthquake (OKADA *et al.*, 1979).

Along the second chain, composed of the Yagi-Yabu and the Mitoke faults, a few large earthquakes occurred. Especially along the Yagi-Yabu fault, the micro-earthquakes are scarce. In contrast, along the Mitoke fault, the micro-seismicity is active (see Fig. 41). Some large earthquakes in the Hokutan block, such as the 1925 Kita-Tajima earthquake of $M6.8$ (UTSU, 1982), are singular. Another pattern of fracture may occur in the coastal region of the Japan Sea.

Along the third chain, composed of the Mikata, the Hanaori and the Ikoma faults, there are many occurrences of large earthquakes for the historical ages. Here, we could include the Obaku, the Ite and the Miyakata faults. The Yamatogawa fault is also involved in this chain. These faults are shown in Fig. 13. This chain can be considered to be the most active chain of the historical seismic events, especially in the segment of the Hanaori fault. Most of the historical earthquakes which occurred in Kyoto City are probably related to the displacement of the Hanaori fault (USAMI, 1987). The 1662 earthquake of $M=7\frac{1}{4}\sim7.6$ is also considered to be caused by the displacement of the Hanaori fault (USAMI, 1987). However, the Hanaori fault seems to become quiet after the 1662 earthquake. Recently, two earthquakes of $M=5$ class occurred at 1979 and 1985 (J.M.A., 1980, 1986). Furthermore, the Hanaori fault causes many micro-earthquakes and makes a boundary of the micro-seismic activity between active and inactive (see Fig. 41).

The Obaku and the Ite faults run in the eastern border of the southern Kyoto basin with an N-S strike (Fig. 13) (R.G.A.F., 1980). The Obaku fault relates to the Hanaori fault as en echelon at Kyoto City and continues to the Ite fault at the south end. Two historical large earthquakes are assumed to be near the Obaku fault.

For the southern segment of this chain, four large historical earthquakes of $M\geqq 6$ occurred along the Ikoma or the Yamatogawa fault. The largest is the 1596 earthquake of $M7.5$. In this segment, the occurrences of large earthquakes cluster around the 16th century, except the 1936 $M6.4$ earthquake.

Along the fourth chain, composed of the Yanagase, the Yoro and the Ise-Bay faults, several large earthquakes were recorded. The Sekigahara fault (Fig. 31) seems to be centered on. Furthermore, an earthquake of $M6.5$ occurred at the north of the Lake Biwa around the Shufukuji or the Yanagase fault.

Along the fifth chain, composed of the Kizugawa fault and the Fujiwaradake or the Suzuka fault, the 1854 earthquake of $M\,7\frac{1}{4}$ occurred and displaced the

Kizugawa fault (USAMI, 1987). Furthermore, the 1819 earthquake of $M\,7\frac{1}{4}$ is considered to be of the Suzuka fault.

Therefore, we could find the most active chain of block boundaries from the Wakasa Bay to face the MTL, although the historical records of earthquakes are centered on Kyoto and its vicinities. This chain is composed of the Mikata, the Hanaori, the Obaku, the Ite, the Ikoma and the Yamatogawa faults and the N-S striking faults to reach the MTL (Fig. 43, Fig. 44, and a detail map shown in Fig. 13). The Yata and the Miyakata faults and the Sabota flexures at the north of Nara are probably included (see Fig. 13). The chain composed of the Yanagase, the Sekigahara, the Yoro and the Ise-Bay faults is also very active (Fig. 43 and Fig. 44). The latter chain is the boundary between the Kinki and the Chubu districts on the tectonic and geologic senses. These two chains play the great roles as stress consumers in the northern Kinki district, central part of Honshu Island. These chains are similar to the two borders of the Kinki triangle of HUZITA (1969). However, the line from the Mikata fault to face the MTL is different than the Osaka Bay-Tsuruga line of HUZITA, especially at both ends of the two lines.

These two chains clearly mark boundaries of the upper crust in the tectonic sense. The depth of the fracture at the block boundary, however, has not been confirmed yet. The blocks between the two chains are the Biwa-ko and the Nara blocks. The basement rocks within the two blocks are mainly granitic rocks. In contrast, the exterior blocks, especially in the northern parts, are mainly composed of old and hard sedimentary rocks as their basements (see Fig. 42). The examples are the Tamba block, the eastern part of the Maizuru block and the undefined east (Mino) block. The activity of intra-block micro-seismicity is higher in the exterior blocks and lower in the Biwa-ko and the Nara blocks (see Fig. 41). The Osaka block, however, shows low activity of intra-block micro-seismicity because of its granitic basement.

6. Conclusions

A combination of geological and geophysical surveys was successful to discover the hidden active faults. The methods employed were the surface geological survey to find the fault outcrops and the distribution of artesian springs along the fault structure, the ELF-magnetotelluric sounding to estimate the resistivity structure, the γ-ray survey to find the fractures at the surface layer, and the gravity method to prospect the vertical displacement of the basement.

The results of the surveys reveal the continuity of major active strike-slip faults in the northern part of Kinki district, southwest Japan. Newly discovered structures are as follows; (1) the Sanda-Yamasaki Tectonic Line (STL) connecting the Yamasaki and the Jumantsuji faults, (2) the Ute fault, which is a candidate for the tectonic

boundary between the Kinki and the Chugoku districts, (3) the connection between the Mitoke and the Yabu-Yagi faults, (4) the fracture zone of the Yagi fault, (5) the southwestern extension of the Yamada fault, (6) the resistivity structures of the Hanaori, the Mikata and the Yanagase faults, (7) the fractures at the northwestern coast of Lake Biwa, and (8) the vertical-slip of the Miyakata fault.

Based on these structures, we can define tentatively the seven tectonic blocks, to the north of the Median Tectonic Line, bounded by the chains of major active faults which often have a strike-slip displacement. The large historical earthquakes, of magnitude above 5.5, are considered to have occurred at these block boundaries.

Two chains of block boundaries are recognized as the most active and the stress-convergence lines: One extends from the Mikata-Hanaori fault to face to the Median Tectonic Line through the Obaku fault and the Ikoma or the Miyakata fault, and the other extends from the Yanagase fault to the Ise-Bay fault through the Yoro fault. The inner region between the two chains has a granitic basement and shows less micro-seismicity. On the contrary, the exterior regions composed of old and hard sedimentary basements show high activity in the intra-block micro-seismicity.

Acknowledgments

This study was carried out under the support of Research Group "Kinki-Kei-hanshin" for Earthquake Prediction and Emeritus Prof. H. MIKI. Parts of the supports owe to Shiga Prefecture, Imazu Town and Ikoma City.

The author is greatly indebted to Prof. S. NISHIMURA for his guidance and advice during the course of this research. The author expresses grateful to Drs. J. NISHIDA, T. MOGI and K. MINO for their critical advice and discussion. The author also thanks Messrs. E.M. ARSADI and Y. YAMADA for their assistance in the field and analytical works, Mr. R. SORKHABI for improving the English, and Miss H. NAKAMURA for drawing the figures.

References

ABE, E. and SASAJIMA, S., (1974): Probable sedimentary thickness in Lake Biwa inferred from the gravity measurements. *in* HORIE, S. *ed. IPPCCE Newsletter,* No. **1,** 2–3.

CAGNIARD, L., (1953): Basic theory of the magneto-telluric method of geophysical prospecting. *Geophysics,* **18,** 605–635.

ELECTROMAGNETIC RESEARCH GROUP FOR THE ACTIVE FAULT (E.R.G.A.F.), (1982): Low electrical resistivity along an active fault, the Yamasaki fault. *J. Geomag. Geoelectr.,* **34,** 103–127.

FUKUI, K., (1981): Fault topography along the Yamasaki fault system, western Kinki district, Japan. *Geograph. Rev. Japan,* **54,** 196–213. (in Japanese with English abstract)

GEOGRAPHICAL SURVEY INSTITUTE (G.S.I.), (1976): Establishment of the Japan Gravity Standardization Net 1975. *J. Geod. Soc. Japan,* **22,** 65–76. (in Japanese with English abstract)

HANDA, S. and SUMITOMO, N., (1985): The geoelectric structure of the Yamasaki and the Hanaori faults, southwest Japan. *J. Geomag. Geoelectr.*, **37,** 93–106.

HANDIN, J., (1966): Strength and ductility. *in* CLARK, S. P., Jr., *ed.* Handbook of Physical Constants-Revised Edition. *Geol. Soc. Am. Mem.*, **97,** 223–289.

HATUDA, Z., (1954): Radioactive method for geological exploration. *Mem. Coll. Sci., Univ. Kyoto,* Ser. B, **21,** 231–271.

HORIE, S. and TANAKA, S., (1983): On the investigation of the lake basin structure by air gun method. *Paleolimn. Lake Biwa Jap. Pleistocene,* **11,** 5–10.

HURUKAWA, N., (1983): P_n velocity and Moho-offset at the west of Lake Biwa in the Kinki district, Japan. *J. Phys. Earth,* **31,** 33–46.

HUZITA, K., (1969): Tectonic development of southwest Japan in the Quaternary period. *J. Geosciences, Osaka City Univ.,* **12,** 53–70.

HUZITA, K., (1974): Quaternary Tectonic Map "Kinki". *Tectonic Map Series* **3,** Geol. Surv. Japan.

HUZITA, K. and KASAMA, T., (1982): Geology of the Osaka-Seihokubu District. *Quadrangle Series, Scale* 1:50,000. Geol. Surv. Japan, 112 pp. (in Japanese with English abstract)

HUZITA, K., KASAMA, T., HIRANO, M., SHINODA, T. and TANAKA-YAMASHITA, M., (1971): Geology and geomorphology of the Rokko area, Kinki district, Japan, with special reference to Quaternary tectonics. *J. Geosciences, Osaka City Univ.,* **14,** 71–124.

HUZITA, K., KISHIMOTO, Y. and SHIONO, K., (1973): Neotectonics and seismicity in the Kinki area, southwest Japan. *J. Geosciences, Osaka City Univ.,* **16,** 93–124.

ICHIKAWA, M., (1971): Reanalyses of mechanism of earthquakes which occurred in and near Japan, and statistical studies on the nodal plane solutions obtained, 1926–1968. *Geophys. Mag.*, **35,** 207–274.

IRIKURA, K. and KAWANAKA, T., (1980): Characteristics of microtremors on ground with discontinuous underground structure. *Bull. Disas. Prev. Res. Inst., Kyoto Univ.,* **30,** 81–96.

ITO, K. and WATANABE, K., (1977): Focal mechanisms of very shallow earthquakes in the vicinity of Lake Biwa. *Zisin (J. Seism. Soc. Japan)*, Ser. 2, **30,** 43–54. (in Japanese with English abstract)

JAPAN METEOROLOGICAL AGENCY (J.M.A.), (1982): Catalogue of relocated major earthquakes in and near Japan (1926∼1960). *Seism. Bull. Japan Meteor. Agency,* Suppl. **6,** 109 pp.

JAPAN METEOROLOGICAL AGENCY (J.M.A.), (1962∼1988): *Seismological Bulletin of Japan Meteor. Agency* for 1961∼1987.

KATSURA, I. and NISHIMURA, S., (1987): Discrimination of γ-ray source, ^{40}K or ^{214}Bi, using γ-ray multichannel pulse-height analyzer. *Zisin (J. Seism. Soc. Japan)*, Ser. 2, **40,** 117–119. (in Japanese)

KATSURA, I., NISHIMURA, S., SADAHIRO, T., MINO, K., MOGI, T. and NISHIDA, J., (1986): γ-ray survey of the Obaku fault, Uji, Japan —Multichannel pulse-height analysis—. *Zisin (J. Seism. Soc. Japan)*, Ser. 2, **39,** 267–275 (in Japanese with English abstract)

KATSURA, I., NISHIMURA, S., ARSADI, E. M., AKAMATSU, S. and MATSUDA, T., (1987a): Tectonic zones in the northwestern part of Kinki district, southwest Japan (5) —The survey of the Yagi fault and the Yamada fault, and the tectonic structure of blocks in the northwestern part of Kinki district—. *Zisin (J. Seism. Soc. Japan)*, Ser. 2, **40,** 561–573. (in Japanese with English abstract)

KATSURA, I., NISHIDA, J. and NISHIMURA, S., (1987b): A computer program for terrain correction of gravity using KS-110-1 topographic data. *Butsuri-Tansa (Geophysical Exploration)*, **40,** 161–175. (in Japanese with English abstract)

KATSURA, I., YAMADA, Y., NISHIMURA, S., MOGI, T., NISHIDA, J. and NAKAO, S., (1989). Tectonic zones at the western-end region of the Yamasaki fault. *Zisin (J. Seism. Soc. Japan)*, Ser. 2, **42,** 341–348. (in Japanese with English abstract)

KAUFMAN, A. A. and KELLER, G. V., (1981): The Magnetotelluric Sounding Method. Elsevier, Amsterdam. 595 pp.

KISHIMOTO, Y., (1981): On precursory phenomena observed at the Yamasaki fault, southwest Japan,

as a test-field for earthquake prediction. *in* SIMPSON, D.W. and RICHARDS, P. G. *eds.*, Earthquake Prediction: An International Review. *Maurice Ewing Volumes* **4,** A.G.U., Washington D.C., 510–516.

KISHIMOTO, Y. and NISHIDA, R., (1973): Mechanisms of microearthquakes and their relation to geological structures. *Bull. Disas. Prev. Res. Inst., Kyoto Univ.,* **23,** 1–25.

KITSUNEZAKI, C., GOTO, N. and IWASAKI, Y., (1971): Underground structure of the southern part of the Kyoto basin obtained from seismic exploration and some related problems of earthquake engineering. *Ann. Disas. Prev. Res. Inst., Kyoto Univ.,* **14-A,** 203–215. (in Japanese with English abstract)

KOBAYASHI, Y., IRIKURA, K., HORIKE, M., AMAIKE, F., KISHIMOTO, K. and KASUGA, S., (1980): Seismic exploration of the Obaku fault. *Ann. Disas. Prev. Res. Inst., Kyoto Univ.,* **23-B,** 95–106. (in Japanese with English abstract)

KOBAYASHI, Y., ANDO, M., IRIKURA, K. and YOSHIZUMI, E., (1984): A geophysical and geological exploration of the Obaku fault, Kyoto. *Zisin (J. Seism. Soc. Japan)*, Ser. 2, **37,** 417–428. (in Japanese with English abstract)

KOIZUMI, N., YOSHIOKA, R., AKAMATSU, S., NISHIMURA, S. and KISHIMOTO, Y., (1986): On hot and mineral springs near the Yamasaki fault. *Ann. Disas. Prev. Res. Inst., Kyoto Univ.,* **29, B-1,** 59–66. (in Japanese with English abstract)

MATSUDA, T., (1975): Magnitude and recurrence interval of earthquakes from a fault. *Zisin (J. Seism. Soc. Japan)*, Ser. 2, **28,** 269–283. (in Japanese with English abstract)

MINO, K., (1984): On a formation mechanism of topography and its relation to earthquake occurrence in southwest Japan. *Bull. Disas. Prev. Res. Inst., Kyoto Univ.,* **34,** 129–167.

MINO, K., (1986): A tectonic zone in the southern part of the Hokuriku district (2) —Sabae fault—. *Zisin (J. Seism. Soc. Japan)*, Ser. 2, **39,** 567–577. (in Japanese with English abstract)

MINO, K. and TAKEUCHI, F., (1977): γ-ray survey around the Obaku fault. *Ann. Disas. Prev. Res. Inst., Kyoto Univ.,* **20-B,** 29–33. (in Japanese with English abstract)

MOGI, T., NISHIMURA, S., MINO, K. and SADAHIRO, T., (1985a): A tectonic zone in the northwestern part of Kinki district, southwest Japan —The Yamasaki fault region—. *Zisin (J. Seism. Soc. Japan)*, Ser. 2, **38,** 57–66. (in Japanese with English abstract)

MOGI, T., MINO, K. and NISHIMURA, S., (1985b): A tectonic zone in the northwestern part of Kinki district, southwest Japan (3) —Yagi-Yabu, Mitoke fault zone—. *Zisin (J. Seism. Soc. Japan)*, Ser. 2, **38,** 577–585. (in Japanese with English abstract)

MOGI, T., MIYOSHI, F., KINOSHITA, K. and ZYOMORI, A., (1986): A geological structure survey by the ELF-MT method at the Zyoso terrace, Ibaraki Prefecture, central Japan. *Butsuri-Tansa (Geophysical Exploration)*, **39,** 139–146. (in Japanese with English abstract)

MURAI, I. and KANEKO, S., (1975): Active fault systems developed in the area around Lake Biwa. *Bull. Earthq. Res. Inst., Univ. Tokyo,* **50,** 93–108. (in Japanese with English abstract)

NISHIDA, J., KATSURA, I. and NISHIMURA, S., (1990): Gravity survey around Lake Biwa, southwest Japan. *J. Phys. Earth,* (submitted).

NISHIDA, R., (1973). Earthquake generating stress in eastern Chugoku and northern Kinki districts, southwest Japan. *Bull. Disas. Prev. Res. Inst., Kyoto Univ.,* **22,** 197–233.

NISHIMURA, S. and KATSURA, I., (1990): Radon in soil gas: Applications in exploration and earthquake prediction. *in* DURRANCE, E. M., GALIMOV, E. M., HINKLE, M. E., REIMER, G. M., SUGISAKI, R. and AUGUSTITHIS, S. S., *eds.*, Geochemistry of Gaseous Elements and Compounds. Theophrastus Pub. S.A., Athens, 497–533.

NISHIMURA, S., MOGI, T., MINO, K. and YAMADA, O., (1985): A tectonic zone in the northwestern part of Kinki district, southwest Japan (2)— The last faulting in the western part of Sanda City, Hyogo Prefecture—. *Zisin (J. Seism. Soc. Japan)*, Ser. 2, **38,** 243–249. (in Japanese with English abstract)

NISHIMURA, S., MOGI, T., AKAMATSU, S. and MATSUDA, T., (1986): A tectonic zone in the northwestern part of Kinki district, southwest Japan (4) —The Yamada fault region—. *Zisin (J. Seism.*

Soc. Japan), Ser. 2, **39,** 371–380. (in Japanese with English abstract)

NOGUCHI, K., (1977): Gravity survey in Seta and Tanakami areas of Otsu City. *Graduate Thesis, Kyoto Univ.*, 15 pp. (in Japanese)

OGAWA, T., TANAKA, Y. and YASUHARA, M., (1969): Schumann resonances and worldwide thunderstorm activity —Diurnal variations of the resonant power of natural noises in the earth-ionosphere cavity—. *J. Geomag. Geoelectr.*, **21,** 447–452.

OGAWA, T., KOZAI, K., KAWAMOTO, H., YASUHARA, M. and HUZITA, A., (1979): Schumann resonances observed with a balloon in the stratosphere. *J. Atmos. Terr. Phys.*, **41,** 135–142.

OHKURA, T., (1988): Focal mechanisms of shallow earthquakes which occurred in San'in, Kinki, and Hokuriku districts. *Zisin* (*J. Seism. Soc. Japan*), Ser. 2, **41,** 89–96. (in Japanese with English abstract)

OIKE, K., (1976): Spatial and temporal distribution of micro-earthquakes and active faults. *Mem. Geol. Soc. Japan,* **12,** 59–73. (in Japanese with English abstract)

OKABE, S., NISHIKAWA, T., NAKAO, S., KISHIMOTO, Y. and KATSURA, I., (1988): γ-ray fluctuation in the observation vault. *25th Ann. Meet. Radioisotopes in Phys. Sci. Industr., Japan.* (in Japanese)

OKADA, A., ANDO, M. and TSUKUDA, T., (1979): Investigation of active faults by trenching. *The Earth Monthly,* **1,** 608–615. (in Japanese)

REDDY, I. K. and RANKIN, D., (1974): Coherence functions for magnetotelluric analysis. *Geophysics,* **39,** 312–320.

REDDY, I. K. and RANKIN, D., (1975): Magnetotelluric response of laterally inhomogeneous and anisotropic media. *Geophysics,* **40,** 1035–1045.

RESEARCH GROUP FOR ACTIVE FAULTS (R.G.A.F.), (1980): Active Faults in Japan, sheet maps and inventories. Univ. Tokyo Press, Tokyo, 363 pp. (in Japanese with English abstract)

SANGAWA, A., (1978): Fault topography and Quaternary faulting along the middle and eastern parts of the Arima-Takatsuki tectonic line, Kinki district, central Japan. *Geograph. Rev. Japan,* **51,** 760–775. (in Japanese with English abstract)

STRANGWAY, D. W., SWIFT, C. M., Jr. and HOLMER, R. C., (1973): The application of audio-frequency magnetotellurics (AMT) to mineral exploration. *Geophysics,* **38,** 1159–1175.

SUDA, S., (1981): Gravity survey in Shigaraki basin, Shiga Prefecture. *Graduate Thesis, Kyoto Univ.*, 59 pp. (in Japanese with English abstract)

SUGIMURA, A., (1963): Notes on the Yanagase fault, Japan. *Quaternary Res. Japan,* **2,** 220–231. (in Japanese with English abstract)

TALWANI, M., WORZEL, J. L. and LANDISMAN, M., (1959): Rapid gravity computations for two-dimensional bodies with application to the Mendocino submarine fracture zone. *J. Geophys. Res.,* **64,** 49–59.

TOGO, M., (1971): Tectonic morphogenesis in the Aibano hill. *Geograph. Rev. Japan,* **44,** 194–200. (in Japanese)

TOGO, M., (1974): Tectonic morphogenesis in the Nosaka mountains, north of Lake Biwa, central Japan. *Geograph. Rev. Japan.* **47,** 669–683. (in Japanese with English abstract)

UEJI, T., (1961): Geology of Kyoto Environs. The Research Institute for Mineral Resources F.J.P., Kyoto, 82 pp. (in Japanese with English abstract)

UEMURA, Y., (1985): Fault topography and Quaternary faulting along the Gomura and Yamada fault systems in the Tango area, central Japan. *Katsudanso-Kenkyu* (*Active Fault Res.*), **1,** 81–92. (in Japanese)

USAMI, T., (1987): Materials for Comprehensive List of Destructive Earthquakes in Japan. Tokyo Univ. Press, Tokyo, 434 pp. (in Japanese)

UTSU, T., (1982): Catalog of large earthquakes in the region of Japan from 1885 through 1980. *Bull. Earthq. Res. Inst., Univ. Tokyo,* **57,** 401–463. (in Japanese with English abstract)

UTSU, T., (1985): Catalog of large earthquakes in the region of Japan from 1885 through 1980 (Correction and supplement). *Bull. Earthq. Res. Inst., Univ. Tokyo,* **60,** 639–642. (in Japanese with English abstract)

VOZOFF, K., (1972): The magnetotelluric method in the exploration of sedimentary basin. *Geophysics,* **37,** 98–141.

WADATSUMI, K. and MATSUMOTO, T., (1958): The stratigraphy of the Neogene formations in northern Tazima —Study of the Neogene in the north-western part of the Kinki district— (Part 1). *J. Geol. Soc. Japan,* **64,** 625–637. (in Japanese with English abstract)

WATANABE, K., MINO, K., NISHIDA, R., MATSUO, S., NAKAO, S. and ENOMOTO, S., (1984): On the seismic activity of Tango Peninsula region (Part 1). *Ann. Disas. Prev. Res. Inst., Kyoto Univ.,* **27, B-1,** 117–124. (in Japanese with English abstract)

YAMADA, N., TERAOKA, Y. and HATA, M. (*Chief eds.*), (1982): Geological map of Japan, scale 1: 1,000,000. *Geological Atlas of Japan,* Geol. Surv. Japan, 3–19, 22–25.

YAMADA, Y., KATSURA, I., NISHIMURA, S. and NISHIDA, J., (1989): Resistivity structure of the Hanaori fault, southwest Japan, using ELF-MT method. *Zisin* (*J. Seism. Soc. Japan*), Ser. 2, **42,** 33–38. (in Japanese with English abstract)